TAMPEREEN TEKNILLINEN YLIOPISTO
TAMPERE UNIVERSITY OF TECHNOLOGY

ANIL BANIYA

ASSESSMENT OF FREQUENCY SELECTIVE SURFACE FOR IMPROVING INDOOR CELLULAR COVERAGE

Master of Science Thesis

Examiner: Professor, Dr. Tech. Mikko Valkama
Supervisor: Ari Asp
Examiners and topic approved by the Faculty Council of the Faculty of Computing and Electrical Engineering on 5th February 2014.

ABSTRACT

TAMPERE UNIVERSITY OF TECHNOLOGY
Master's Degree Programme in Electrical Engineering
BANIYA, ANIL: Assessment of frequency selective surface for improving indoor cellular coverage
Master of Science Thesis, 68 pages, 2 Appendix pages
February 2014
Major: Radio Frequency Electronics
Examiner: Professor Dr. Tech. Mikko Valkama
Supervisor: Ari Asp
Keywords: Frequency Selective Surface, Transmission, Indoor coverage, GSM, UMTS

Modern houses use energy efficient building materials like metal shielding and energy saving windows to improve the thermal efficiency. Such energy efficient building materials creates the barrier for outdoor-to-indoor RF signals propagation which is one of the challenging problems in the field of cellular communication. In order to solve such problem of outdoor-to-indoor propagation, an effective and efficient solution is very essential. Some existing techniques to solve the indoor coverage problem are the use of outdoor to indoor repeaters, pico-cell or dedicated indoor systems like distributed antenna system and radiating cables. However, such techniques are operator oriented; expensive for single residential houses; possess additional network architecture design and maintenance complexity. One of the newer passive techniques which is operator independent and does not have additional network burden, is the use of frequency selective windows. Frequency selective windows consist of Frequency Selective Surface (FSS) etched on the metal coating of the energy saving windows, allowing cellular frequencies to pass through them while blocking the thermal radiation. FSS is the combination of either conducting patches or apertures in a thin conducting sheet arranged periodically in one or two dimensional array. FSS possess frequency selective behavior based on the element geometry. Patch type of FSS exhibits total reflection around resonant frequency whereas aperture type exhibits total transmission.

This thesis presents the modelling, simulation, fabrication and test measurements of the FSS that is transparent to GSM and UMTS frequency band. FSS with a double square loop aperture as a unit cell is selected for the analysis. The modelling and simulation of the FSS are carried out in the Computer Simulation Technology (CST) microwave studio, 2012 version. FSS prototype is fabricated using the commercial available aluminum foil. Furthermore, the FSS prototype is tested in the laboratory as well as in real-time networks. The real-time or field measurement is conducted in the real networks for all three operators of Finland, namely DNA, Elisa and TeliaSonera. The laboratory result shows the resonant frequency shift downwards by a factor of 1.22 comparing to the simulation results of freestanding FSS. The reason behind such frequency shift is well explained by the presence of a dielectric substrate in FSS prototype. On average, for all operators the field measurement result shows the transmission improvement of around 10 dB and 4.5 dB in GSM and UMTS band respectively over the plain aluminum foil. Although the field measurement result does not show much improvement compared to the laboratory measurement result, it still prevails the possibility of using FSS for indoor coverage improvement.

PREFACE

This thesis has been done for the completion of Master of Science Degree in Electrical Engineering at Tampere University of Technology, Tampere, Finland. The research work has been carried out in the Department of Electronics and Communication Engineering under Digital Transmission Group during the year 2013 to 2014.

First of all, I would like to thank my examiner Professor Mikko Valkama for providing me the thesis topic and fund for this research. I express my sincere gratitude to my supervisor Ari Asp for his continuous guidance, suggestions and valuable feedbacks throughout this work. I should not forget to thank my colleague Mikko Keskikastari for helping me during the measurement campaign. I would also like to thank my friends Dipesh Poudel, Prakash Subedi, Nirajan Pant and Udhyan Timilsina for their support and encouragement during my thesis work; special thanks to Sandeep Kumar Shrestha.

I am indebted to my parents and sisters for their unconditional love and continuous support throughout my life. Finally, I would like to dedicate this thesis to my Late grandfather Mr. Nar Bahadur Baniya.

Tampere, July 2014

Anil Baniya
baniyanil@gmail.com

CONTENTS

LIST OF ABBREVIATIONS

2G	Second Generation
3G	Third Generation
3GPP	Third Generation Partnership Project
AGCH	Access Grant Channel
ARFCN	Absolute Radio Frequency Channel Numbers
AuC	Authentication Centre
BCCH	Broadcast Control Channel
BCH	Broadcast Channel
BPL	Building Penetration Loss
BSC	Base Station Controller
BSS	Base Station Subsystem
BTS	Base Transceiver Station
CCCH	Common Control Channel
CCH	Control Channel
CN	Core Network
CPCH	Common Packet Channel
CPICH	Common Pilot Channel
CS	Circuit Switched
CST	Computer Simulation Technology
CTCH	Common Traffic Channel
DAS	Distributed Antenna System
dB	Decibel
DCCH	Dedicated Control Channel
DCH	Dedicated Channel
DPCCH	Dedicated Physical Common Channel
DPDCH	Dedicated Physical Data Channel
DSCH	Downlink Shared Channel
DSSS	Direct Sequence Spread Spectrum
DTCH	Dedicated Traffic Channel
EGSM	Extended GSM
EIR	Equipment Identity Register
EM	Electromagnetic
ETSI	European Telecommunications Standards Institute
EU	European Union
FACCH	Fast Associated Control Channel
FACH	Forward Access Channel
FCCH	Frequency Correction Channel
FDD	Frequency Division Duplexing
FHMA	Frequency Hopped Multiple Access
FIT	Finite Integration Technique

FSS	Frequency Selective Surfaces
GGSN	Gateway GPRS Support Node
GMSC	Gateway Mobile Switching Centre
GPRS	General Packet Radio Service
GSM	Global System for Mobile Communications
HLR	Home Location Register
HS-DSCH	High Speed Downlink Shared Channel
IMEI	International Mobile Equipment Identity
IPCC	International Panel on Climate Change
ISDN	Integrated Services Digital Network
LNA	Low Noise Amplifier
LTE	Long Term Evolution
MAC	Media Access Control
Mcps	Megachips per second
ME	Mobile Equipment
MS	Mobile Station
MSC	Mobile Switching Centre
NSS	Network and Switching Subsystem
NZEL	Nearly Zero-Energy Level
OMC	Operation and Maintenance Centre
OSS	Operation Support Subsystem
PBC	Periodic Boundary Condition
PCCH	Paging Control Channel
P-CCPCH	Primary Common Control Physical Channel
PCH	Paging Channel
P-CPICH	Primary Common Pilot Channel
PEC	Perfect Electric Conductor
PICH	Paging Indicator Channel
PLMN	Public Land Mobile Network
PRACH	Physical Random Access Channel
PS	Packet Switched
PSTN	Public Switched Telephone Network
QoS	Quality of Service
RACH	Random Access Channel
RACH	Random Access Channel
RF	Radio Frequency
RNC	Radio Network Controller
RRM	Radio Resource Management
RSCP	Received Signal Code Power
RSSI	Received Signal Strength Indicator
RX	Receiver
SACCH	Stand-Alone Dedicated Control Channel

S-CCPCH	Secondary Common Control Physical Channel
SCH	Synchronization Channel
S-CPICH	Secondary Common Pilot Channel
SGSN	Serving GPRS Support Node
SIM	Subscriber Identity Module
TCH	Traffic Channel
TDMA	Time Division Multiple Access
TE	Transverse Electric
TEM	Transverse Electromagnetic
TM	Transverse Magnetic
TS	Time Slot
TX	Transmitter
UE	User Equipment
UMTS	Universal Mobile Telecommunication System
USIM	Universal Subscriber Identity Module
UTRAN	Universal Terrestrial Radio Access Network
VLR	Visitor Location Register
WCDMA	Wideband Code Division Multiple Access

LIST OF SYMBOLS

ε	Permittivity [F/m]
ε_0	Permittivity of free space [F/m]
ε_r	Relative Permittivity
μ	Permeability [H/m]
μ_0	Permeability of free space [H/m]
μ_r	Relative Permeability
ρ_s	Scattering loss factor
ρ_s	Surface charge density [C/m^3]
θ_i	Angle of Incident
θ_r	Angle of reflection
θ_t	Angle of transmission
σ	Conductivity [S/m]
Γ	Reflection coefficient
τ	Transmission coefficient
α	Attenuation constant [Np/m]
β	Phase constant [rad/m]
γ	Complex propagation constant [1/m]
δ	Skin depth [m]
η	Wave impedance [Ω]
λ	Wavelength [m]
ρ	Electric charge density [C/m^3]
ω	Angular frequency [rad/s]
$\boldsymbol{B}$	Magnetic flux density [Wb/m^2]
$\boldsymbol{D}$	Electric flux density [C/ m^2]
$\boldsymbol{E}$	Electric field intensity [V/m]
f	Frequency [Hz]
$\boldsymbol{H}$	Magnetic field intensity [A/m]
$\boldsymbol{J}$	Electric current density [A/m^2]
$\boldsymbol{J}_s$	Surface current density [A/m^2]
k	Propagation constant or Wave number [1/m]
$\boldsymbol{P}$	Poynting vector [W/ m^2]
v_p	Phase velocity [m/s]
Y_L	Load admittance
Z_L	Load impedance

LIST OF FIGURES

LIST OF TABLES

1. INTRODUCTION

The climate change has resulted in the global warming referring to the continuous rise in the average temperature of the earth's climate system. According to International Panel on Climate Change (IPCC), one of the main reasons behind global warming is the emission of carbon dioxide from fossil fuel combustion, cement production and the deforestation. Thus, this global warming has driven human to lower level of carbon dioxide and other fossil fuels as a source of energy. European Union (EU) has made its strategic priority to prevent the dangerous climate change. The member countries are working hard to cut its greenhouse gases emission substantially while encouraging other nations as well. For this reduction, EU leaders have committed for transforming Europe into a high energy-efficient, low carbon economy. For 2020, EU has committed to cutting its greenhouse gas emission to 20% below 1990 levels. In the climate and energy policy framework for 2030, the European Commission has set a target of lowering the emission to 40% below 1990 levels by 2030. [1.]

Housing, which is one of the basic needs of humans, consumes a lot of natural resources during the construction phase. At the same time, heating and cooling systems used in households are another major share of energy. Especially in the northern countries where the winter is rather long and cold, heating systems consumed most of the energy. Around 70% of total household energy consumption is contributed by the heating system, which leads to about 14% of EU greenhouse gas emissions [2]. Thus, to reduce the energy consumption in the heating system, EU mandates that all new constructed buildings need to achieve so-called Nearly Zero-Energy Level (NZEL) by 2021 [3]. In the context of this thesis, zero-energy houses, which is also, commonly known as low-energy houses or passive-energy houses refer to the houses which have high energy efficiency in terms of thermal isolation properties.

To meet the EU's target of zero-energy houses, modern houses are expected to use more energy-efficient construction materials. Metal has very good properties which provide better means of achieving a high level of thermal isolation. Hence using metals in the modern building construction materials has become popular to achieve the energy-efficiency requirements. These modern building materials, therefore, may consist of metal-based insulation boards and energy saving windows. Energy saving windows has a very thin layer of metallic coating to ensure the thermal isolation. On the other hand, metal as an insulator generates the problem with Radio Frequency (RF) signals. All modern wireless communication technologies use RF signals for communication, which cannot propagate well through a metal shielding.

Considering building materials of walls, like bricks, wood, masonry block, rock and concrete, windows allow the easiest way for radio signals to enter into buildings. It is because the attenuation caused by glass windows is not more than few decibels (dBs) [4, see 5]. However, if those windows are replaced with energy efficient windows, the radio signal attenuation increases considerably. The report [4] and research [5] show the attenuation of RF signals caused by the modern construction materials. This means, in modern houses, exterior walls and windows clearly create a barrier for efficient propagation of RF signals into the buildings.

A high portion of cellular traffic originates from inside of buildings. Around 70% to 80% of mobiles are used indoor and users demand a good coverage and Quality of Service (QoS) for indoor use. Therefore, operators are also showing an increasing interest in the field of indoor radio reception and planning. Number of research has been done for improving the indoor radio coverage. Some of the existing techniques for improving indoor coverage are outdoor-to-indoor repeater, picocell (small cell) and dedicated indoor coverage with distributed antenna systems and radiating cables. However, such techniques are expensive for single residential houses, possess design and maintenance complexity, and increase additional network configuration. The other possible solutions to overcome the indoor coverage problem can be achieved by modifying the modern building construction materials. One passive way to improve the indoor coverage is to adding RF holes with some conducting materials into the building which can couple RF energy on intended frequencies. Another passive method to improve the indoor mobile coverage can be arranged by using Frequency Selective Surface (FSS) in energy efficient windows or other construction materials. Such passive technology to improve indoor coverage without additional network configuration has been proposed in [6-10].

FSS is an array of conducting patch or aperture conducting elements which possess the frequency selective behavior [11]. Due to the frequency selective nature, FSS acts like electromagnetic filters. Based on the element geometry (patch or aperture), FSS may have low- pass or high-pass frequency response. FSS can be designed properly to exhibit total transmission or reflection around the resonant frequency. FSSs are used in radomes (antenna covers) to reduce the radar cross section of antennas outside their operating band. Therefore, such radomes are widely used in missiles, aircraft and ships for military uses. FSSs are also used in filter applications like band-pass filters, dichroic sub-reflectors, polarizers and beamsplitters. Besides these applications, FSS finds its application in recent wireless communication fields for frequency selective windows.

The objective of this thesis is to investigate the use of FSS for improving indoor cellular coverage. FSS with double square loop aperture element is selected for the analysis purpose. Double square loop aperture element behaves like a double band-pass filter. So the frequency response of FSS is tuned to cover both frequency bands of Global System for Mobile (GSM) and Universal Mobile Telecommunication System (UMTS) cellular networks. GSM and UMTS are most common cellular networks than Long Term Evolution (LTE) network because LTE network is new in today's cellular market. LTE network covers different range of frequency bands which increase the complexity in de-

signing shape of FSS's unit cell element. Hence, to reduce the complexity in FSS prototype fabrication this thesis only focuses on GSM and UMTS cellular networks. Finally, FSS prototype was fabricated and tested in real network of three operators of Finland which include DNA, Elisa and TeliaSonera. The frequency response of FSS for DNA (GSM 900 and UMTS 2100), Elisa (GSM 1800 and UMTS 2100) and Teliasonera (GSM 900 and UMTS 2100) are measured and analyzed.

The entire thesis is divided into eight chapters. Chapter 1 is the introduction itself which includes the motivation and objective of the whole research. Chapter 2 provides an insight into fundamentals of the electromagnetic theory. Furthermore, Chapter 3 provides the overview of GSM and UMTS as cellular mobile technology. Different mechanisms of radio wave propagation along with the indoor coverage techniques are discussed in chapter 4. Moreover, the theory behind FSS and its designed criteria and simulation software used for the simulation of FSS are described in chapter 5 and 6 respectively. The simulations results are also presented in the chapter 6. Chapter 7 contains the laboratory as well as real time measurement of fabricated FSS. After laboratory measurement, constructed FSS was further tested in the real network for its reliability in real life. Both measurement results are presented in this chapter. Finally, the thesis is concluded in chapter 8 with the overall summary of the thesis.

2. BASIC ELECTROMAGNETIC THEORY

Electromagnetic (EM) waves were first proposed by James Clerk Maxwell in 1873 and later confirmed by Heinrich Hertz in 1888 [12]. An EM wave consists of both electric and magnetic fields oscillating perpendicularly to each other and to the direction of propagation. Electromagnetic theory is indispensable for the understanding of FSS theory since it deals with the propagation of radio waves through it. Radio waves or RF waves refer to the waves whose frequency ranges from 30 kHz to 300 GHz in EM spectrum [13]. In today's world, RF waves find its application in the fields of wireless communications systems, radar systems, environmental remote sensing, medical systems and many more. Some important topics in electromagnetic theory for better understanding of EM waves are discussed in the following sub-chapters.

2.1. Maxwell's Equation

The well-known four sets of Maxwell's equations, which was named after James Clerk Maxwell completely describes the electric and magnetic phenomena of the wave. The oscillation of electric and magnetic energy generates the EM waves. It is also responsible for the wave propagation. The time differential forms of Maxwell's equations are [14]

$$\nabla \times \boldsymbol{E} = -\frac{\partial \boldsymbol{B}}{\partial t}, \tag{2.1}$$

$$\nabla \times \boldsymbol{H} = \frac{\partial \boldsymbol{D}}{\partial t} + \boldsymbol{J}, \tag{2.2}$$

$$\nabla \cdot \boldsymbol{D} = \rho, \tag{2.3}$$

$$\nabla \cdot \boldsymbol{B} = 0, \tag{2.4}$$

where **E** is the electric field intensity (V/m), **H** is the magnetic field intensity (A/m), **D** is the electric flux density (C/m^2), **B** is the magnetic flux density (Wb/m^2), $\boldsymbol{J}$ is the electric current density (A/m^2) and ρ is the electric charge density (C/m^3). With the help of these equations, Maxwell derived a wave equation which gives that the EM wave travels with the same velocity of light [14].

Equation (2.1) is known as Faraday's law which says that the time varying magnetic field generates the electric field circulating around it. Equation (2.2) is the modified form of Ampere's circuital law. Ampere's circuital law [$\nabla \times \boldsymbol{H} = \boldsymbol{J}$] which says the curl of magnetic field is equal to the electric current density. Later Maxwell found the problem that Ampere's circuital law is violating the principle of charge conservation in time varying case. So he added a new term, displacement current density ($\partial \boldsymbol{D}/\partial t$) to fulfil

the principle of charge conservation. Hence, the modified equation, which is also, known as Ampere-Maxwell law says that a flowing electric current gives rise to a rotational magnetic field. Continuity equation, which can be, derived from the Ampere-Maxwell law is expressed as

$$\nabla \cdot \boldsymbol{J} = -\frac{\partial \rho}{\partial t}, \tag{2.5}$$

which gives the principle of conservation of charge. Continuity equation states that charge can neither be created nor destroyed. The net flow of current inside or outside a certain volume must be equal to rate of decrease or increase of the charge inside that volume [14]. Equations (2.3) and (2.4) are the Gauss's law of electrostatic and Gauss's law of magnetism respectively. Gauss's law of electrostatic states the divergence of the electric flux density gives the total electric charge density, and Gauss's law of magnetism states that the magnetic fields are solenoid (circulating) since magnetic charge (monopole) does not exist.

The two constitutive properties of the medium are [14]

$$\boldsymbol{B} = \mu \boldsymbol{H} = \mu_r \mu_0 \boldsymbol{H}, \tag{2.6}$$
$$\boldsymbol{D} = \varepsilon \boldsymbol{E} = \varepsilon_r \varepsilon_0 \boldsymbol{E}, \tag{2.7}$$

where μ and ε are permeability and permittivity of medium; μ_r and ε_r are the relative permeability and relative permittivity of medium respectively whose corresponding free space values are given as $\mu_0 = 4\pi \times 10^{-7}$(H/m) and $\varepsilon_0 = 8.854 \times 10^{-12}$(F/m) [14].

2.2. Boundary Condition

Often the electromagnetic problems involve different media with different physical properties. So it is necessary to know the conditions of field quantities **E**, **D, H, B** at the interface of the two media. The set of boundary condition equations can be summarised as follows [14; 15; 16]

$$\boldsymbol{a_n} \times (\boldsymbol{E}_2 - \boldsymbol{E}_1) = 0, \tag{2.8}$$
$$\boldsymbol{a_n} \times (\boldsymbol{H_2} - \boldsymbol{H_1}) = \boldsymbol{J_s}, \tag{2.9}$$
$$\boldsymbol{a_n} \cdot (\boldsymbol{D}_2 - \boldsymbol{D}_1) = \rho_s, \tag{2.10}$$
$$\boldsymbol{a_n} \cdot (\boldsymbol{B}_2 - \boldsymbol{B}_1) = 0. \tag{2.11}$$

In the above equations, index 1 and 2 denotes the field quantities in media 1 and 2 respectively. Here, a_n is the unit normal vector to the boundary surface and is pointing from media 1 to media 2. The cross products of the unit normal vector with the field quantities form the tangential components to the boundary. According to the equations (2.8) and (2.9), the tangential component of the electromagnetic field at the boundary is

continuous ($\boldsymbol{E}_{1t} = \boldsymbol{E}_{2t}$), and the tangential component of magnetic field is discontinuous at the interface where a surface current exist and the amount of discontinuity is equal to the surface current density ($\boldsymbol{H}_{2t} = \boldsymbol{H}_{1t} + \boldsymbol{J}_s$).

Similarly, the dot products of unit normal vector with the field quantities form the normal components to the boundary. Equation (2.10) says that the normal component of the electric flux density is discontinuous at the media interface where a surface charge exists, and the amount of discontinuity is equal to the surface charge density ρ_s, which is equals to $\boldsymbol{D}_{2n} - \boldsymbol{D}_{1n}$. Equation (2.11) says that the normal component of magnetic flux density is continuous at the interface ($\boldsymbol{B}_{1n} = \boldsymbol{B}_{2n}$).

2.3. Wave Equation

Wave propagation problems often concerned the performance of an EM wave in a source-free region where ρ and *J* are both zero. In a simple (linear, isotropic and homogeneous) non-conducting medium characterized by ε and μ (σ = 0), Maxwell's equations can be solved to give a second-order equation as [14]:

$$\nabla^2 \boldsymbol{E} - \mu\varepsilon \frac{\partial^2 \boldsymbol{E}}{\partial t^2} = 0, \tag{2.12}$$

$$\nabla^2 \boldsymbol{H} - \mu\varepsilon \frac{\partial^2 \boldsymbol{H}}{\partial t^2} = 0. \tag{2.13}$$

These are the homogeneous vector wave equation. For the time-harmonic case, phasor form of Maxwell's equations can be solved to derive the wave equations. For source-free and linear medium, the wave equations also known as homogeneous vector Helmholtz equations are represented as [14]

$$\nabla^2 \boldsymbol{E} + k^2 \boldsymbol{E} = 0, \tag{2.14}$$

$$\nabla^2 \boldsymbol{H} + k^2 \boldsymbol{H} = 0, \tag{2.15}$$

where $k = \omega\sqrt{\mu\varepsilon}$ is the propagation constant or wave number in the medium. ω is the angular frequency.

2.4. Plane Waves

Several different solutions of the wave equations (2.12) and (2.13) or (2.14) and (2.15) represent waves. The simplest solution is the uniform plane wave which has one-dimensional spatial dependence. It means if a uniform plane wave propagates along some fixed direction (say z-direction) its electric and magnetic field has no dependence on the transverse coordinates *x* and *y*, but are functions of coordinate *z* and time *t* only. A uniform plane wave is a transverse electromagnetic (TEM) wave, meaning electric and magnetic fields are perpendicular to each other and are propagating to the direction

which is perpendicular to both of them [14]. A source infinite in extent is needed to create a uniform plane wave which is practically impossible. However, far enough from the source, waves become almost spherical and a very small portion of a large spherical wave is approximately a plane wave.

2.4.1. Plane Waves in Lossless Media

Considering only one field component (*x*-component of the electric field) propagating in the *z* direction and no variation of this field in *x*- and *y*-directions, equation (2.14) reduces to [14]

$$\frac{\partial^2 \boldsymbol{E}_x}{\partial z^2} + k^2 \boldsymbol{E}_x = 0. \tag{2.16}$$

The solution of this equation is given as

$$\boldsymbol{E}_x(z) = E^+ e^{-jkz} + E^- e^{jkz}. \tag{2.17}$$

In the time domain,

$$\boldsymbol{E}_x(z,t) = E^+ \cos(\omega t - kz) + E^- \cos(\omega t + kz). \tag{2.18}$$

In the right hand side of the equation (2.18), the first term is the wave travelling in the +*z* direction and the second term in the –*z* direction. E^+ and E^- are arbitrary amplitude constants. The phase velocity is given by

$$v_p = \frac{\omega}{k} = \frac{1}{\sqrt{\mu\varepsilon}}. \tag{2.19}$$

With similar assumption for electric field component, magnetic field can be calculated as [14]

$$\boldsymbol{H}_y(z,t) = \frac{1}{\eta}\boldsymbol{E}_x(z,t), \tag{2.20}$$

where $\eta = \sqrt{\mu/\varepsilon}$ is the wave impedance for the plane wave and is defined as the ratio of electric and magnetic field.

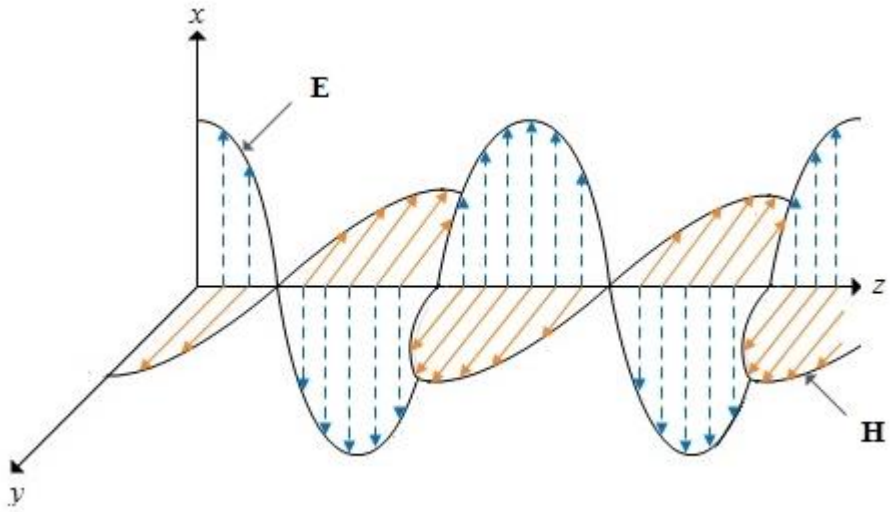

Figure 2.1. *A uniform electromagnetic plane wave propagating in +z direction at time t [17].*

Figure 2.1 shows a uniform electromagnetic plane wave propagating in +z direction. The blue line and the brown line show the electric field and the magnetic field respectively, which are perpendicular to each other.

2.4.2. Plane Waves in Lossy Media

For lossy media, the wavenumber *k* in equations (2.14) and (2.15) becomes a complex number because permittivity for lossy media is complex. Hence the wave equations represented by equations (2.14) and (2.15) can be written as [14]

$$\nabla^2 \boldsymbol{E} + k_c^2 \boldsymbol{E} = \nabla^2 \boldsymbol{E} - \gamma^2 \boldsymbol{E} = 0, \tag{2.21}$$

$$\nabla^2 \boldsymbol{H} + k_c^2 \boldsymbol{H} = \nabla^2 \boldsymbol{H} - \gamma^2 \boldsymbol{H} = 0, \tag{2.22}$$

where γ is the complex propagation constant defined as

$$\gamma = jk_c = j\omega\sqrt{\mu\varepsilon_c} = \alpha + j\beta, \tag{2.23}$$

where $\varepsilon_c = \varepsilon + \frac{\sigma}{j\omega} = \varepsilon' - j\varepsilon''$ is the complex permittivity, α is the attenuation constant which gives the rate of decay with distance and β is the phase constant which expresses the amount of phase shift that occurs as the wave travels a distance of one meter.

Thus, the complex propagation constant can be expressed as [14]

$$\gamma = j\omega\sqrt{\mu\varepsilon}\sqrt{1 + \frac{\sigma}{j\omega\varepsilon}}. \tag{2.24}$$

For lossless media, $\sigma = 0$ and $\alpha = 0$, so $\beta = k = \omega\sqrt{\mu\varepsilon}$.

Assuming only *x*-component of the electric field, the wave equation reduces to

$$\frac{\partial^2 \boldsymbol{E}_x}{\partial z^2} - \gamma^2 \boldsymbol{E}_x = 0, \tag{2.25}$$

which has a solution

$$\boldsymbol{E}_x(z) = E^+ e^{-\gamma z} + E^- e^{\gamma z}. \tag{2.26}$$

Here, $e^{-\gamma z} = e^{-\alpha z} e^{-j\beta z}$ gives the wave travelling in $+z$ direction with exponential damping factor $e^{-\alpha z}$, where z is the distance in meter. It means the field strength of the travelling wave diminishes exponentially in a lossy medium. The associated magnetic field is given by

$$\boldsymbol{H}_y(z) = \frac{-j\gamma}{\omega\mu}(E^+ e^{-\gamma z} - E^- e^{\gamma z}). \tag{2.27}$$

The wave impedance for lossy medium is

$$\eta = \frac{j\omega\mu}{\gamma}. \tag{2.28}$$

2.4.3. Plane Waves in Good Conductors

For a good conductor: $\sigma/\omega\varepsilon >> 1$ [16]. Hence, the complex propagation constant can be written as

$$\gamma = \alpha + j\beta \cong j\omega\sqrt{\mu\varepsilon}\sqrt{\frac{\sigma}{j\omega\varepsilon}} = \frac{1+j}{\sqrt{2}}\sqrt{\omega\mu\sigma} = (1+j)\sqrt{\frac{\omega\mu\sigma}{2}}, \tag{2.29}$$

which implies

$$\alpha = \beta = \sqrt{\frac{\omega\mu\sigma}{2}} = \sqrt{\pi f\mu\sigma}. \tag{2.30}$$

Equation (2.30) shows, attenuation constant is directly proportional to frequency (*f*). It means that the high frequency EM wave is attenuated more rapidly as it propagates in a good conductor. Since the attenuation factor is $e^{-\alpha z}$, the amplitude of the wave will be attenuated by a factor of $e^{-1} = 0.368$ when it travels a distance of $z = \delta = 1/\alpha$. The distance δ is called the skin depth or depth of penetration and given as

$$\delta = \frac{1}{\alpha} = \frac{1}{\sqrt{\pi f\mu\sigma}}. \tag{2.31}$$

This distance δ is very small for a good conductor at radio wave frequencies. Hence a thin sheet of good conductor (e.g. silver, gold, copper or aluminium) can significantly block the transmission of radio waves through them [14; 16].

2.5. Polarization of Plane Waves

Polarization of plane waves can be defined as the orientation of the electric field vector as a function of time at a given point in space. A plane wave propagating in +*z*-direction consist of the electric field and magnetic field varying along x- and y-axes with respect to time. These electric and magnetic fields are always perpendicular to each other. Therefore, polarization of the plane waves can be explained only with electric field behaviour and a separate description of magnetic field behaviour is not necessary [14]. Suppose, the plane wave travelling along +*z*-direction consists of the following electric filed components $\boldsymbol{E}_x$ and $\boldsymbol{E}_y$ along *x*- and *y*-axes respectively. Then,

$$\boldsymbol{E}_x = E_1 \cos(\omega t - kz), \tag{2.32}$$
$$\boldsymbol{E}_y = E_2 \cos(\omega t - kz + \delta), \tag{2.33}$$

where E_1 and E_2 are the magnitude of electric field along *x*- and *y*-axes respectively and δ is the phase difference between $\boldsymbol{E}_x$ and $\boldsymbol{E}_y$. Hence the instantaneous electric field $\boldsymbol{E}$ can be written as

$$\boldsymbol{E} = \boldsymbol{E}_x\bar{x} + \boldsymbol{E}_y\bar{y} = E_1 \cos(\omega t - kz)\bar{x} + E_2 \cos(\omega t - kz + \delta)\bar{y}. \tag{2.34}$$

The plot of the equation (2.34) leads to the formation of an ellipse as shown in Figure 2.2.

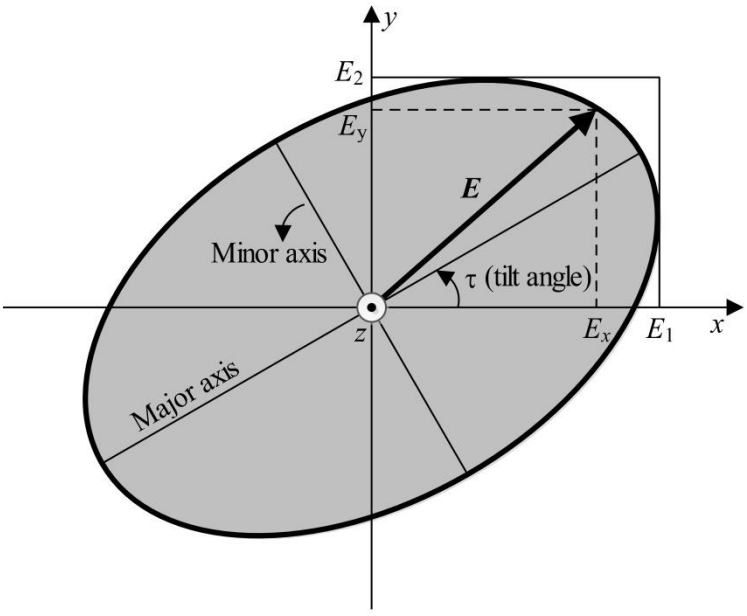

Figure 2.2. *Polarization ellipse; z-axes is pointing out of the paper [18].*

There are three different types of polarization namely linear, circular and elliptical as shown in Figure 2.3, Figure 2.4 and Figure 2.5.

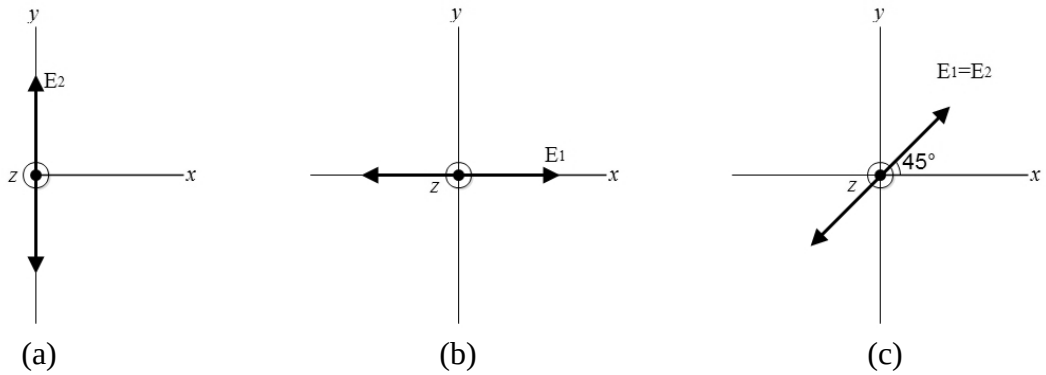

(a) (b) (c)

Figure 2.3. *Linear Polarization. (a) Vertical (b) Horizontal (c) Slanted [19].*

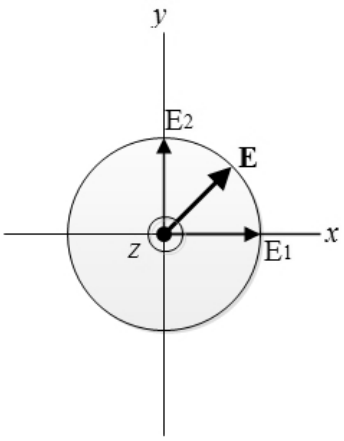

Figure 2.4. *Circular Polarization [19].*

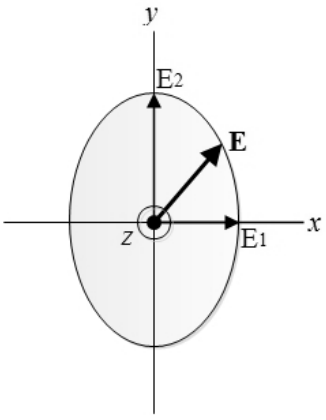

Figure 2.5. *Elliptical Polarization [19].*

Linear and circular polarisations are the special cases of elliptical polarization which are described below,

- If $E_1 = 0$, the wave is linearly polarized in *y*-axes and it is called vertical polarization which is shown in Figure 2.3(a).
- If $E_2 = 0$, the wave is linearly polarized in *x*-axes and it is called horizontal polarization which is shown in Figure 2.3(b).
- If $E_1 = E_2$ and $\delta = 0$, the wave is still linearly polarized but tilted at $\tau = 45^o$ as shown in Figure 2.3(c).
- If $E_1 = E_2$ and $\delta = \pm 90^o$, wave is circularly polarized and is shown in Figure 2.4.

2.6. Power Transfer and Poynting Theorem

Electromagnetic waves carry electromagnetic power within them. Poynting theorem gives a relation between the power transfer and the electromagnetic field associated with a travelling wave. Poynting theorem can be expressed as [14]:

$$\oint_S (\boldsymbol{E} \times \boldsymbol{H}) \cdot dS = -\frac{\partial}{\partial t}\int_V (\frac{1}{2}\epsilon \boldsymbol{E}^2 + \frac{1}{2}\mu \boldsymbol{H}^2) dV - \int_V \sigma \boldsymbol{E}^2 dV . \qquad (2.35)$$

In equation (2.35), the first integral in the right hand side is the total time rate of change of the energy stored in electric and magnetic field and the second integral is the total ohmic power dissipated in the volume. As according to the law of charge conservation, the total sum of the expression on the right hand side must be equal to the power leaving the volume through its surface. Thus, the quantity on the left hand side ($\oint_S (\boldsymbol{E} \times \boldsymbol{H}) \cdot dS$) is the power leaving the volume and the quantity $\boldsymbol{E} \times \boldsymbol{H}$, is the power flow per unit area denoted by $\boldsymbol{P}$. Here the quantity $\boldsymbol{P}$ is known as pointing vector. The direction of Poynting vector ($\boldsymbol{P}$) is always normal to both electric and magnetic field and gives the direction of power flow.

3. CELLULAR MOBILE TECHNOLOGY

This thesis investigates the use of FSS in the improvement of indoor coverage for Global System for Mobile communication (GSM) and Universal Mobile Telecommunication System (UMTS). So this chapter includes a brief introduction of GSM and UMTS cellular technology.

3.1. GSM

GSM is the first digital cellular mobile technology which belongs to second generation (2G) [20]. GSM was developed to solve the fragmentation problems of the first cellular systems in Europe [20]. Before GSM, many countries in Europe were using different standards which make single subscriber unit incompatible throughout the Europe. Thus, GSM was originally established with the goal of creating European standard for cellular communication. In mid-1980s, GSM committee specify a common mobile communication platform for Europe in 900 MHz band. Later in 1992, GSM changed its name to Global System for Mobile communications for marketing purpose [20]. Success of GSM could not be confined only within Europe; hence it became the world's popular standard.

3.1.1. GSM Architecture

The system architecture of GSM consists of three major interconnected subsystems which are Base Station Subsystem (BSS), Network and Switching Subsystem (NSS) and Operation Support Subsystem (OSS) as illustrated in Figure 3.1. The Mobile Station (MS) is also a subsystem, but is usually considered as a part of the BSS for architecture purposes. These subsystems interact between themselves and with the users through different network interfaces like A interface, Abis interface and Um interface. Um interface is the also known as radio air interface which is of more concern in context of this thesis. The brief description of each GSM architecture element is presented in the following sub-chapters.

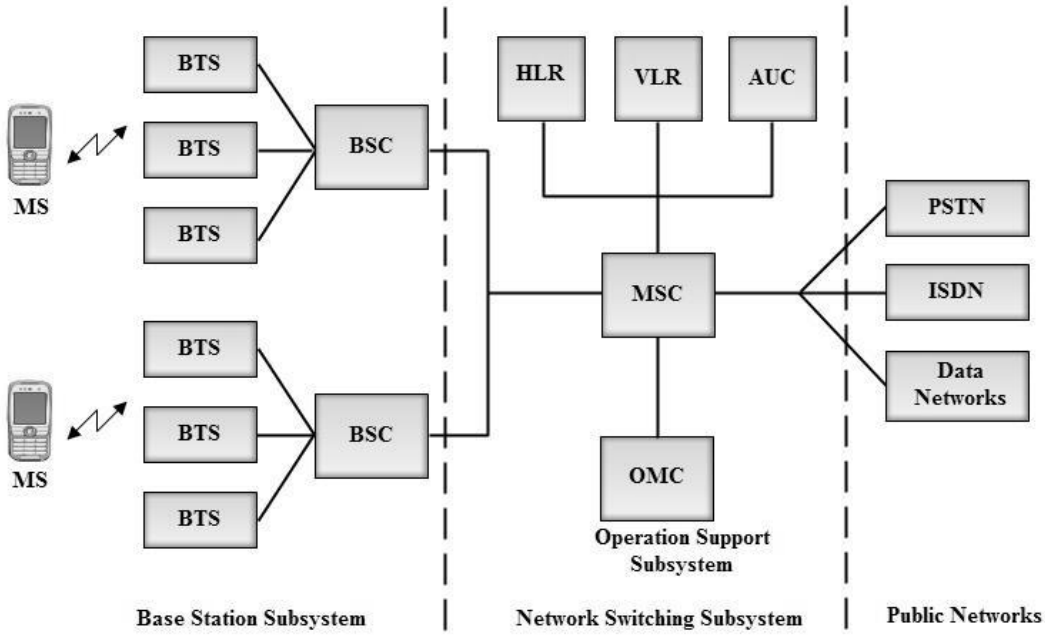

Figure 3.1. *GSM Architecture [20].*

3.1.1.1 BSS

The BSS, which is also, known as radio subsystem contains the equipment to manage radio interface between MS and other subsystems of GSM. It mainly consists of Base Station Controller (BSC), Base Transceiver Station (BTS) and MS. There can be several BTSs connected to one BSC which communicates with MSs via radio air interface. BSC handles the handovers related to its own controlled BTSs. Each MS contains a memory chip called Subscriber Identity Module (SIM) which stores user's identification number, the networks and other user-specific information.

3.1.1.2 NSS

The NSS includes the equipment which handles end-to-end call, management of subscriber, mobility and interface with public networks such as Public Switched Telephone Network (PSTN) and Integrated Services Digital Network (ISDN). The NSS consists of different equipment such as Mobile Switching Centre (MSC), Visitor Location Register (VLR), Home Location Register (HLR) and Authentication Centre (AuC). The function of MSC is to provide call setup, routing, handover between base stations and interface to public fixed networks. The HLR is a centralized database of all subscribers registered in the network. The VLR is a database of all subscribers currently roaming in MSC's control area. AuC handles the authentication and encryption keys for each single subscriber in the HLR and VLR. Auc also contains the Equipment Identity Register (EIR) which stores International Mobile Equipment Identity (IMEI) numbers of all registered mobile equipment.

3.1.1.3 OSS

The OSS consists of Operation and Maintenance Centre (OMC) which monitor and performs maintenance of GSM equipment. Beside this, OSS also manages all charging and billing procedures.

3.1.2. Frequency Planning

Originally GSM was specified as a 900 MHz system which is also called as the standard or primary GSM900 band. This primary GSM900 band includes two sub-bands of 25 MHz each separated by 45 MHz frequency band for uplink (MS to BTS) and downlink (BTS to MS) transmission. The frequencies from 890 MHz to 915 MHz were assigned for uplink and from 935 MHz to 960 MHz for downlink. Later the GSM frequency band was extended to EGSM900 and GSM1800 to increase the capacity. The EGSM band is the extended band which also includes primary GSM900 band. The frequency plan for GSM900, EGSM900 and GSM1800 as standardised by European Telecommunications Standards Institute (ETSI) [24] are shown in Table 3.1.

Table 3.1. *GSM Frequency Bands.*

System	Frequency band (MHz)	
	Uplink	**Downlink**
GSM900	890-915	935-960
EGSM900	880-915	925-960
GSM1800	1710-1785	1805-1880

3.1.3. GSM Channel Types

The GSM uses FDD (Frequency Division Duplexing) and combination of TDMA (Time Division Multiple Access) and FHMA (Frequency Hopped Multiple Access) schemes to provide multiple accesses to mobile users [20]. The uplink and downlink frequency bands in GSM are divided into 200 kHz wide channels called Absolute Radio Frequency Channel Numbers (ARFCNs). Hence, there are all together 125 channels (without guard band) within each uplink and downlink frequency band. Each channel, in the time domain, is divided into eight unique Timeslots (TSs) using TDMA. Only one subscriber can use one TS at a time, so each channel supports as many as eight subscribers. The combination of TS number and ARFCN constitutes a physical channel [20]. The physical channel carries either traffic data, signalling data or control channel data. Each physical channel can be mapped to logical channel at different times. The radio sub-system in GSM supports two logical channels: Traffic Channels (TCHs) and Control Channels (CCHs) [25].

3.1.3.1 Traffic Channels (TCHs)

The traffic channels are the channels that carry digitally encoded speech or user data both in uplink and downlink directions. According to their traffic rates, TCHs are categorized into full rate traffic channel (TCH/F) and half rate traffic channel (TCH/H). The TCH/F and the TCH/H carry the information at a gross rate of 22.8 kbps and 11.4 kbps respectively [25]. The TCH/F can support the speech at the rate of 13 kbps or user data at the rate of 2.4 kbps (TCH/F2.4), 4.8 kbps (TCH/F4.8) or 9.6 kbps (TCH/F9.6). Similarly, TCH/H supports the speech at 6.5 kbps or data at 2.4 kbps (TCH/H2.4) or 4.8 kbps (TCH/H4.8).

3.1.3.2 Control Channels (CCHs)

Control channels are intended to carry signalling or synchronization data. CCHs are divided into three main categories, and they are Broadcast Channel (BCH), Common Control Channel (CCCH) and Dedicated Control Channel (DCCH).

- *Broadcast channel (BCH)*:
  BCH is further divided into three channels: Broadcast Control Channel (BCCH), Frequency Correction Channel (FCCH) and Synchronization Channel (SCH). BCCH operates only in downlink direction and broadcasts information such as cell/network identity, system information and channel availability, required for MS to operate efficiently. FCCH allows each MS to synchronize its internal frequency to BS. SCH is used to identify the serving BTS and for frame synchronization of the mobile to BTS.
- *Common control channel (CCCH)*:
  CCCH consists of three different channels: Paging Channel (PCH), Random Access Channel (RACH) and Access Grant Channel (AGCH). PCH is the downlink channel used to provide paging signals, alerting mobile for incoming calls. RACH is uplink channel used to acknowledge a page from the PCH and to initiate a call. AGCH is the downlink channel used to assign dedicated channel to mobile. This channel is also used by BS to respond RACH send by a mobile.
- *Dedicated control channel (DCCH):*
  DCCH is a bi-directional channel that works on both uplink and downlink directions. DCCH is categories into three channels: Stand-alone Dedicated Control Channel (SDCCH), slow associated control channel (SACCH) and Fast Associated Control Channel (FACCH). SDCCH is used for providing signalling services required by the mobiles. SACCH and FACCH are used to supervise data transmissions between mobile station and base station during a call. In downlink direction, SACCH is used to send slow but regularly changing control information like transmit power level instruction. While in uplink direction, it carries information about the received signal strength [20].

3.1.4. Mobility Management

In GSM network, management of service quality and mobility is very important as it keeps track of users in move. The network must provide the best possible service quality and handover to the users. Handover is the procedure where active MS switches the BTS which has the best service quality. The MS measures the signal strength levels and quality of the BCH of the serving cell, as well as of neighbouring cells. The MS informs these measurement reports to the BS. Meanwhile, the BS also measures the signal strength level and quality of the received signal from the MS. Based on these measurements, BSC manages the handover and service quality. The signal strength of the received radio waves is measured as Rx-Level and is reported in a range from 0 to 64. Rx-Level 0 is: -110 dBm and Rx-Level 64 is: -46 dBm [21].

3.2. UMTS

The UMTS is the third generation (3G) cellular mobile technology developed to overcome the data limitations of 2G networks. 3G system was designed for multimedia communication enhanced by higher data rates. It offers the theoretical data rates up to 2 Mbps, seamless mobility for voice and packet data applications, Quality of Service (QoS) and simultaneous voice and data capability [26]. Wideband Code Division Multiple Access (WCDMA) has emerged as the most widely adopted 3G air interface in the standardisation forums [26]. UMTS uses WCDMA as access technique to offer high spectral efficiency and bandwidth. The specification of UMTS was standardized by 3rd Generation Partnership Project (3GPP) from Released 99 [26; 27].

3.2.1. UMTS Architecture

The system architecture of UMTS inherits most of the GSM network elements and functional principles. The only remarkable change is in the development of new radio access part of the network. Based on the functionality of network elements, the architecture of UMTS is divided into three domains: User Equipment (UE), Universal Terrestrial Radio Access Network (UTRAN) and Core Network (CN). The system architecture of UMTS along with associated elements is shown in Figure 3.2.

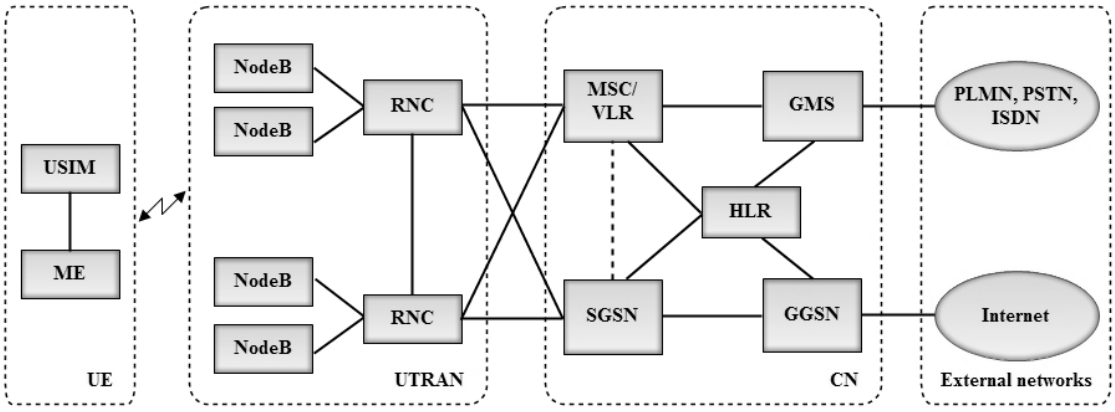

Figure 3.2.*UMTS architecture [26].*

3.2.1.1 UE

The UE is the user end device which consists of Mobile Equipment (ME) and Universal Subscriber Identity Module (USIM). ME is the radio terminal used for radio communication and USIM is a memory chip which stores the subscriber information along with authentication and encryption keys. The UE is similar to MS in GSM network.

3.2.1.2 UTRAN

UTRAN handles all the radio-related functionality and is similar to BSS in GSM network. UTRAN consists of two important network elements namely NodeB and Radio Network Controller (RNC). NodeB which is equivalent to BTS in GSM network handles the user physical data and signalling between UE and RNC. The RNC manages the radio resources of all the NodeBs that are connected to it. It is equivalent to BSC of GSM network.

3.2.1.3 CN

The CN is responsible for switching and routing calls and data connections to external networks. According to the nature of traffic handled, the elements of CN can be divided into two domains, Packet-Switched (PS) and Circuit-Switched (CS) domains [27]. The CS domain consists of network elements like MSC/VLR, Gateway MSC (GMSC), HLR, AuC and EIR. The GMSC forms a gateway between CN of the UMTS and external networks like PSTN, ISDN and PLMN (Public Land Mobile Network). The function of MSC/VLR is similar to that of GSM network and capable of handling both 2G and 3G subscribers. PS domain is an evolved General Packet Radio Service (GPRS) system which comprises the network elements like Serving GPRS Support Node (SGSN) and Gateway GPRS Support Node (GGSN). The function of SGSN is to handle the data packets between the subscribers. It is also responsible for mobility management, authentication and billing. The GGSM forms a gateway between PS domain and external network like internet.

3.2.2. Frequency Allocation

As standardized by 3GPP release 99, the UMTS/FDD is allocated the frequency band around 2 GHz. In Europe, the frequency band for uplink is 1920-1980 MHz and 2110-2170 MHz for downlink [26]. The uplink and downlink directions are separated by different frequencies, and the duplex distance is 190 MHz [41]. WCDMA utilizes the Direct Sequence Spread Spectrum (DSSS) technique to spread the air interface, with a system chip rate of 3.84 Mcps (Megachips per second) leading to a radio channel of 5 MHz bandwidth. The system chip rate is the bit rate of the code used for spreading the original signal.

3.2.3. UMTS Channel Types

The radio channel in UMTS is divided into three categories: logical channels, transport channels and physical channels [27]. Logical channels describe the types of transmitted information; transport channels describe how these logical channels are to be transferred; and physical channels are the transmission media which provide the radio platform to transfer actual information.

3.2.3.1 Logical Channels

Logical channels are not real channels; rather they can be understood as different tasks the network and the UE need to carry out at different times. Logical channels are mapped to the transport channels in Media Access Control (MAC) layer. The different types of logical channels are described below.

- *Broadcast Control Channel (BCCH)*: This channel broadcasts system control information such as code value(s) used in own cell and neighbour cells, allowed power levels etc. in downlink direction.
- *Paging Control Channel (PCCH)*: It transfers paging information in downlink direction. Paging information may contain the command to discover UE exact location.
- *Common Control Channel (CCCH)*: It transfers the common control information for all the UE within its cell. It can be used in both uplink and downlink directions.
- *Dedicated Control Channel (DCCH)*: It transfers the control information concerning particular connection while UE is in active mode.
- *Dedicated Traffic Channel (DTCH)*: It carries user data for particular UE in uplink and downlink directions.
- *Common Traffic Channel (CTCH)*: It is used to broadcast the data to a group of UE in downlink direction.

3.2.3.2 Transport Channels

The different types of transport channels, which are interface, between physical and MAC layer are described below.

- *Broadcast Channel (BCH)*: It carries the content of the BCCH.
- *Paging Channel (PCH)*: It carries paging information to establish the connection with UE in the downlink direction.
- *Forward Access Channel (FACH)*: It carries control information or user data to UE in the downlink direction.
- *Dedicated Channel (DCH)*: It transfers the dedicated control and user data in both directions.
- *Downlink Shared Channel (DSCH)*: It carries dedicated user information (DTCH and DCCH) for packet data and can be shared by several users.
- *High Speed DSCH (HS-DSCH)*: It is similar to DSCH but with enhanced data capability.
- *Random Access Channel (RACH)*: It is used to send control information from UE in the uplink direction.
- *Common Packet Channel (CPCH)*: It is a common transport channel intended for packet data transmission in uplink direction.

3.2.3.3 Physical Channels

The physical channels are used between the UE and the NodeB. The transport channels are mapped to different physical channels which are described below.

- *Primary Common Control Physical Channel (P-CCPCH)*: It is responsible to carry system information in BCH in downlink directions.
- *Secondary Common Control Physical Channel (S-CCPCH)*: This physical channel carries two transport channels (PCH and FACH) within it.
- *Paging Indicator Channel (PICH)*: It is used to carry the paging indicators.
- *Dedicated Physical Data Channel (DPDCH)*: It carries dedicated user data in both directions.
- *Dedicated Physical Common Channel (DPCCH)*: It transfers control information during the active connection.
- *Physical Random Access Channel (PRACH)*: It carries the RACH transport channel.
- *Synchronisation Channel (SCH)*: It provides the cell search information for the UE located within the cell range.
- *Common Pilot Channel (CPICH)*: It is used by UE for dedicated channel estimation and to provide channel estimation reference when common channels are involved. CPICH is downlink channel broadcast by NodeBs with constant power. Typically 10% of the total downlink power is assigned to CPICH [21]. The CPICH is divided into two pilot channels: Primary CPICH (P-CPICH) and Secondary CPICH (S-CPICH). There is only one P-CPICH per cell and is transmit-

ted over the entire cell. However, there can be zero, one or several s-CPICH per cell, which are, transmitted over the entire cell or only over a part of the cell.

3.2.4. Mobility Management in UMTS

Efficient utilisation of the air interface resources can be done by the Radio Resource Management (RRM) algorithms. RRM is responsible to maintain the QoS and high capacity throughout the coverage area. RRM can be divided into handover control, power control, admission control, load control and packet scheduling functionalities [26]. Mobility of UE across the cell boundaries is managed by the handover control mechanism. For the handover decision, the UE measures Received Signal Code Power (RSCP), Received Signal Strength Indicator (RSSI) and E_c/N_o from the P-CPICH [26]. RSCP is the received power on one code after dispreading, defined on the pilot symbols. It is used to evaluate handover decision, downlink open loop control, signal to interference ratio (SIR) and path loss. Similarly, RSSI is the wide-band received power within the channel bandwidth and is used to evaluated inter system handover (UMTS to GSM). E_c/N_o is the ratio of received energy per chip of the pilot channel to the total noise power density. In other words, it is also defined as RSCP/RSSI and used for handover evaluation purpose. [26; 27.]

3.3. Radio Frequency Allocation in Finland

This thesis includes the measurement of indoor received signal strength through FSS for three commercial network operators of Finland. These three commercial network operators are DNA, TeliaSonera and Elisa. According to the Finnish Communications Regulatory Authority, the allocations of radio frequency bands for these network operators are shown in Table 3.2, Table 3.3 and Table 3.3 [28]. Åland is the Swedish-speaking Island of Finland where the frequency allocation is exceptional than the whole country which is also shown in the tables.

Table 3.2. *900 MHz frequency band.*

Operators	Uplink (MHz)	Downlink (MHz)	Technology
DNA	800.1 – 891.7 (nationwide except Åland)	925.1 – 936.7 (nationwide except Åland)	GSM/UMTS
TeliaSonera	891.9 – 903.3 (nationwide except Åland) 885.1 – 902.3 (Åland)	936.9 – 948.3 (nationwide except Åland) 930.1 – 947.3 (Åland)	
Elisa	903.5 – 914.9 (nationwide except Åland)	948.5 – 959.9 (nationwide except Åland)	

Table 2.2 shows the frequency band allocation around 900 MHz. The frequency bands are divided into uplink and downlink bands. All the shown operators can use GSM or UMTS as the cellular mobile technology around 900 MHz frequency band.

Table 3.3. *1800 MHz frequency band.*

Operators	Uplink (MHz)	Downlink (MHz)	Technology
TeliaSonera	1710.1 – 1734.9 (nationwide)	1805.1-1829.9 (nationwide)	GSM/UMTS /LTE
DNA	1735.1 – 1759.9 (nationwide except Åland)	1830.1 – 1854.9 (nationwide except Åland)	
Elisa	1760.1 -1784.9 (nationwide except Åland)	1855.1 – 1879.9 (nationwide except Åland)	

Table 2.3 shows the frequency band allocation around 1800 MHz. It also shows operators are allowed to use GSM or UMTS or LTE technology at 1800 MHz band. Table 2.4 shows the frequency allocation for the three operators around 2 GHz.

Table 3.4. *2 GHz frequency band.*

Operators	Uplink (MHz)	Downlink (MHz)	Technology
Elisa	1920.3 – 1940.1 (nationwide except Åland) 1935.3 – 1950.1 (Åland)	2110.3 – 2130.1 (nationwide except Åland) 2125.3 – 2140.1 (Åland)	GSM/UMTS /LTE
DNA	1940.1 – 1959.9 (nationwide except Åland)	2130.1 – 2149.9 (nationwide except Åland)	
TeliaSonera	1959.9 – 1979.7 (nationwide except Åland) 1964.9 – 1979.7 (Åland)	2149.9 – 2169.7 (nationwide except Åland) 2154.9 – 2169.7 (Åland)	

4. RADIO WAVE PROPAGATION

In cellular network system, the transmitted radio wave reaches the receiving station by propagating through different environment. This propagating environment in cellular network terms is also known as radio channel. The basic physical mechanisms (reflection, diffraction and scattering) that are responsible for the propagation of EM waves in radio channel are discussed in sub-chapters.

4.1. Reflection and Transmission

Reflection of the radio wave occurs when it encounter a smooth obstacle whose dimensions are significantly large than the wavelength of the incident wave. For example, such objects can be ground surface, buildings or the walls. If the radio wave propagating in one medium incident on the second medium having different electrical properties, part of its energy is transmitted into second medium and part of the energy gets reflected back to first medium. If the radio wave strikes the perfect dielectric materials, some energy is reflected back and some energy is transmitted without any loss. But if the second medium is a perfect conductor, all the energy is reflected back without any loss. For indoor propagation, transmission of radio wave is important. It is because either the base station is located outside or inside the building the wave has to penetrate the walls and floors before reaching the receiver. Reflection of radio wave primarily depends on conductivity and permittivity of the reflecting surface, as well as the angle of incidence, polarization and frequency of the incident wave [20].

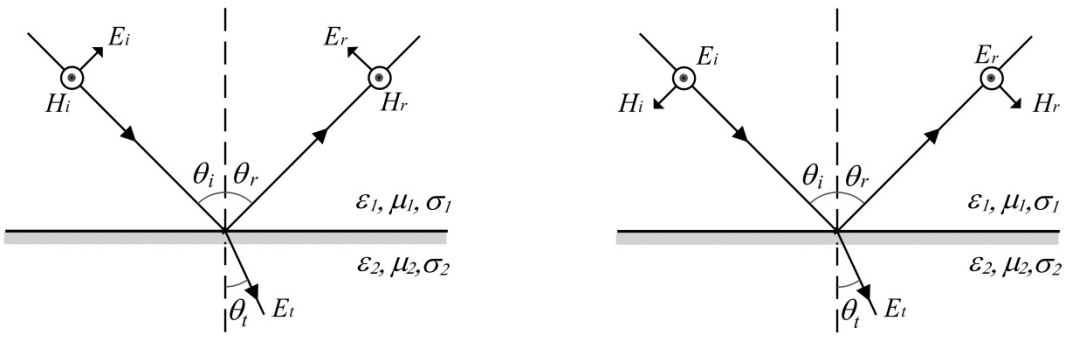

Figure 4.1. *Reflection and Transmission of plane wave. (a) TM polarization (b) TE polarization [20].*

Figure 4.1 shows the polarized EM wave incident at an angle θ_i to the surface normal at the point of incidence. Some of the incident wave gets reflected back to the same

medium making an angle of reflection θ_r to the normal and some gets transmitted into the second medium making an angle of transmission θ_t. In Figure 4.1, the subscripts *i*, *r*, *t* refers the incident, reflected, and transmitted fields. Parameters ε_1, μ_1, σ_1 and ε_2, μ_2, σ_2 represent the permittivity, permeability and conductance of the media 1 and 2 respectively. A polarized EM wave can be decomposed into two orthogonal polarizations namely Transverse Electric (TE) and Transverse Magnetic (TM) polarization. A polarization state where the electric field component (*E*) is parallel to the plane of incidence is known as TM (also known as vertical or parallel) polarization as shown in Figure 4.1 (a). Similarly, if the electric field component is perpendicular to the plane of incidence it is known as TE (or horizontal or perpendicular) polarization as shown in Figure 4.1 (b). [20; 29.]

Now according to Snell's law, the incident angle is equal to the reflected angle ($\theta_i = \theta_r$) and incident angle is linked to the transmitted angle (θ_t) by the following equation [17; 30]:

$$\frac{\sin\theta_t}{\sin\theta_i} = \frac{\sqrt{\varepsilon_1\mu_1}}{\sqrt{\varepsilon_2\mu_2}}. \tag{4.1}$$

Reflection coefficient is defined as the ratio of reflected wave to the incident wave. Similarly, transmission coefficient is the ratio of the transmitted wave to the incident wave.

As according to [17; 31], for TE polarisation,

$$\Gamma = \frac{E_r}{E_i} = \frac{\eta_2\cos\theta_i - \eta_1\cos\theta_t}{\eta_2\cos\theta_i + \eta_1\cos\theta_t}, \tag{4.2}$$

$$\tau = \frac{E_t}{E_i} = \frac{2\eta_2\cos\theta_i}{\eta_2\cos\theta_i + \eta_1\cos\theta_t}. \tag{4.3}$$

For TM polarisation,

$$\Gamma = \frac{E_r}{E_i} = \frac{\eta_1\cos\theta_i - \eta_2\cos\theta_t}{\eta_2\cos\theta_t + \eta_1\cos\theta_i}, \tag{4.4}$$

$$\tau = \frac{E_t}{E_i} = \frac{2\eta_1\cos\theta_i}{\eta_2\cos\theta_t + \eta_1\cos\theta_i}, \tag{4.5}$$

where Γ is the reflection coefficient; τ is the transmission coefficient; η_1 and η_2 are the intrinsic impedance of media 1 and media 2 respectively.

4.2. Diffraction

Diffraction occurs when the radio wave encounter the obstacles which has sharp irregular surfaces (edges/wedges) and has the dimension larger than the signal wavelength. Propagation of radio waves around the curved earth's surface, beyond the horizon and behind the obstructions like hills and tall buildings is due to the diffraction phenome-

non. In practice, obstructed (shadowed) region are never completely sharp, and some energy still propagates into the shadow region. The strength of radio waves decreases as we move deeper in the shadowed region, but it still has enough strength to yield a useful signal. This phenomenon of diffraction can be understood from Huygen's principle, which states that each point of a wavefront can be considered as point source for the production of secondary wavelets, and they combine to produce a new wavefront in the direction of propagation [29]. As a result, diffracted wave is produced by the propagation of secondary wavelets in the shadowed region. Thus, the vector sum of the electric field components of all the secondary wavelets gives the field strength of diffracted wave.

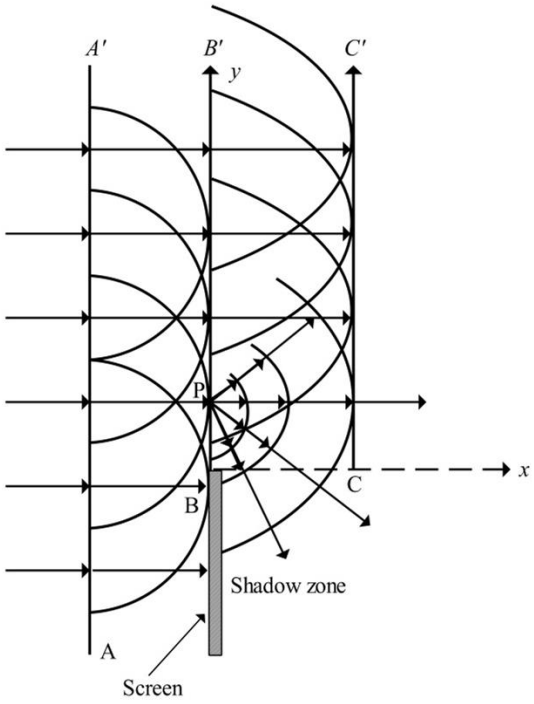

Figure 4.2. *Illustration of Huygen's principle [29].*

Figure 4.2 demonstrates the diffraction phenomenon at the edge of an obstacle following Huygen's principle. The straight line A'A represents the infinite wavefront of incoming radio wave. Each point of this wavefront produces the secondary wavelets (semi-circles) to form new wavefront represented by the straight line B'B. If the wavefront encounters an obstacle, which eliminates parts of the point source of wavefront B'B, only a semi-infinite wavefront C'C exits. Hence according to Huygen's principle wavelets produced from each point of B'B (suppose P) propagate into the shadow region.

4.3. Scattering

Scattering occurs when the propagating wave encounter the objects whose dimensions are small compared to the wavelength of the wave. Scattered waves are formed by rough surfaces or small objects. Radio wave gets reflected in a specular direction when

it impinges on a smooth surface. But when the surface becomes progressively rougher, the reflected wave spread in all directions due to scattering as illustrated in Figure 4.3. This reduces the energy in the specular direction and increases the energy in other directions.

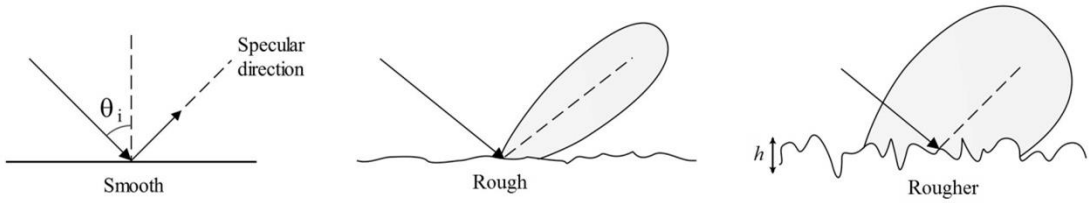

Figure 4.3. *The effect of surface roughness on reflection [31].*

The degree of scattering depends on the roughness of the surface, incident angle (θ_i) and wavelength of the incident wave. A roughness of the surface can be estimated using Rayleigh criterion as given by equation (4.6)

$$h_c = \frac{\lambda}{8sin\theta_i}. \tag{4.6}$$

According to this criterion, the surface is considered rough if the height of surface bumps is less than h_c. For rough surface, the reduction of the reflected field can be accounted by multiplying the corresponding reflection coefficient (Γ) by the scattering loss factor (ρ_s). For the surface height h and standard deviation about the mean surface σ_h, scattering loss factor is given as [20]

$$\rho_s = exp\left[-8\left(\frac{\pi\sigma_h \sin\theta_i}{\lambda}\right)^2\right]. \tag{4.7}$$

Hence for rough surface (h>hc), the reflection coefficient will be

$$\Gamma_{rough} = \rho_s\Gamma. \tag{4.8}$$

4.4. Multipath Propagation

Multiple replicas of the transmitted radio wave arrive at the receiver through different paths due to the phenomenon such as reflection, diffraction and scattering, as shown in Figure 4.4. These multipath signal components have random phase and amplitudes. Thus, the multiple signal components can combine constructively or destructively at the receiver. If the two received signals are in-phase with each other, they combine constructively to amplify the overall received signal and if they are out-of-phase, the overall signal weakens. But if the phase difference between two received signals is 180°, they cancel each other resulting in no reception of the transmitted wave. As the signal propagates through different paths before reaching the receiver, the signals will arrive at dif-

ferent time intervals. Thus, signal spreading can occur in time (as well as frequency) resulting in delay spread. Delay spread is the time between the first and the last received multipath component.

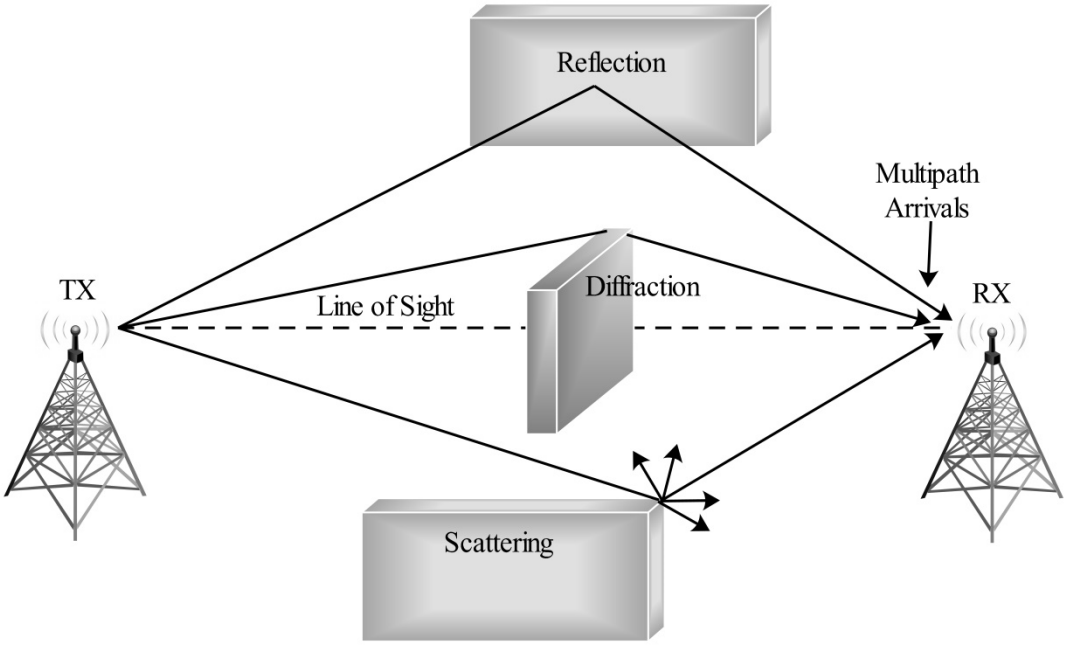

Figure 4.4. *Multipath phenomenon [33].*

Figure 4.4 shows the multipath phenomenon where received signal arrivals via reflection, diffraction and scattering. If there are no obstacles between transmitting (TX) and receiving (RX) antenna, then there exists a strong line of sight component which is represented by a straight dotted line.

4.5. Indoor Cellular Coverage

The number of users in a cellular network has been increasing day by day. Most of the users spend their maximum time inside the buildings such as home, office and shopping malls. Research has shown, in many countries the number of indoor users are about 80% [21]. That is why; the indoor cellular coverage is gaining importance in today's network planning. It is the responsibility of network operators to provide sufficient coverage, capacity and QoS to serve indoor users. The traditional approach of outdoor-to-indoor coverage is discussed as below:

4.5.1. Outdoor-to-indoor Coverage

Basically, outdoor networks (macro cell/micro cell) are designed not only to cover outdoor users but also indoor users within the range. To meet the increasing indoor users demand, special care should be taken while planning outdoor network. One way to improve the indoor coverage is to enhance the outdoor networks by increasing site density.

Although the outdoor signal penetrates the building, its strength becomes very weak due to the high attenuation imposed by the building materials. The attenuation caused by the building materials is known as Building Penetration Loss (BPL). Such losses could be handled in link budget while planning outdoor network. The link budget gives the relationship between transmitted power and signal strength. Hence it requires high transmission power and/or high outdoor site density to have adequate indoor coverage. This leads to the coverage overlapping of outdoor networks increasing interference.

Beside outdoor-to-indoor coverage, indoor cellular coverage can be improved in other methods also. Some of these methods include outdoor-to-indoor repeater or dedicated indoor system connected to an antenna, distributed antenna system or radiating cable.

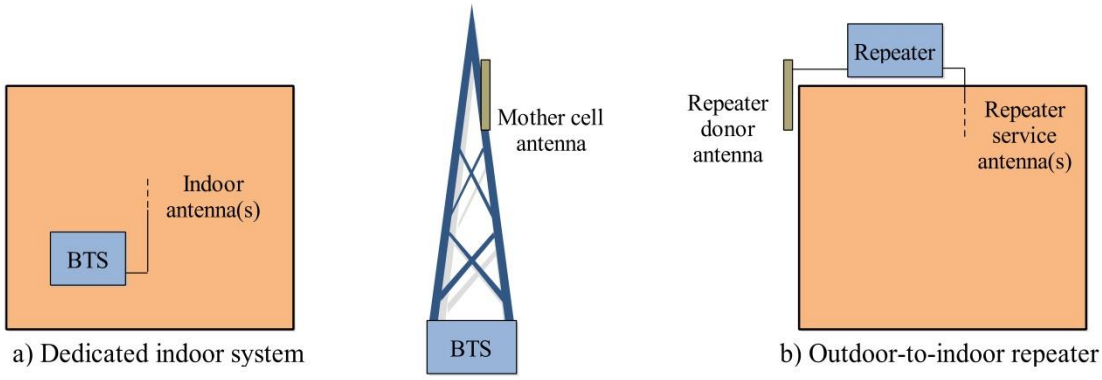

Figure 4.5. *Basic approaches of outdoor-to-indoor coverage [34].*

Figure 4.5 (a) shows the basic configuration of dedicated indoor system and Figure 4.5 (b) shows outdoor-to-indoor repeater system. Further, dedicated indoor system can be implemented by two strategies. One is to have a single BS for one building known as single cell strategy and other to have multiple BS in one building known as multi-cell strategy. These two dedicated indoor system strategies will be discussed more in section 4.5.5 and 4.5.6. Likewise, the outdoor-to-indoor repeater system will also be discussed in section 4.5.4.

4.5.2. Distributed Antenna System (DAS)

DAS consists of several antenna elements connected to a single base station. The basic idea of DAS is to distribute the radio frequency (RF) signal uniformly among the antennas, separated is space, to provide smooth coverage typically in the indoor environment. There are mainly two approaches to implement DAS: Passive DAS and Active DAS [31]. Passive antenna line elements such as coaxial cable, signal splitters or tappers, signal combiners and attenuators are used to distribute the signal in passive DAS. If the losses in the passive DAS become prominent, active amplification can be used to overcome such losses. Such system with active RF components is known as active DAS. Uplink reception can be improved by adding low noise amplifier (LNA) closest to the

antenna to reduce the overall system noise figure while downlink amplification is easy with centralized BTS [31; 34].

4.5.3. Radiating Cable

The radiating cable, commonly known as leaky feeder is the special type of coaxial cable with tuned slots in the outer shield as shown in Figure 4.6 [31]. Such cable acts as a long antenna or actually small antennas radiating along the cable length. Traditionally, radiating cables were used to provide uniform coverage in underground tunnels and coal mines [31]. However, nowadays it has been used to provide coverage inside the buildings which has long corridors, emergency staircases or elevator shafts where coverage with traditional antenna is difficult.

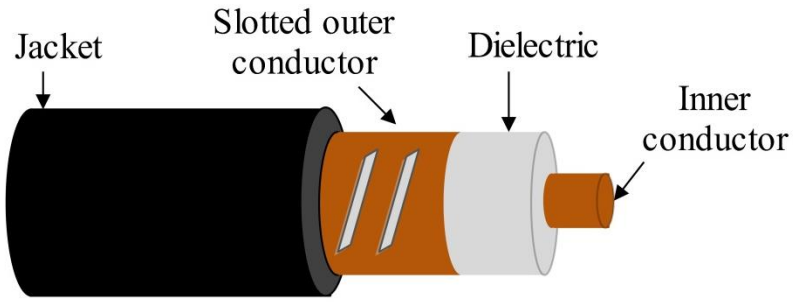

Figure 4.6. *Radiating cable [31].*

4.5.4. Outdoor-to-indoor Repeater

A repeater is a bi-directional amplifier that receives the radio signals and transmits the amplified radio signals. Repeaters are used to improve the reception of signal level where coverage is poor. Typically, repeater consists of three functional units namely service antenna line, amplifier unit and donor antenna line. In outdoor-to-indoor repeater configuration, repeater's donor antenna receives the signal from the mother cell, amplifies and retransmits it inside the building via service antenna. The RF signal received by the repeater can be distributed inside the building using DAS or radiating cables or the combination of both. This type of repeater configuration helps to overcome the BPL, improving the indoor coverage. There should be sufficient isolation between the donor antenna and service antenna for a repeater to function effectively.

4.5.5. Single Cell Strategy

Picocell or small cell is formed when a base station is located inside a building [31]. Picocell in a cellular network provides good coverage for the small area such as in-building offices, shopping malls or train stations. Single cell strategy consists of, one indoor BTS to cover a building. As long as the BPL is high, the outdoor BTSs interference always remains low. Indoor coverage could be made better by implementing DAS and radiating cables to the single cell strategy [34]. The single cell strategy along with

DAS and radiating cables is shown in Figure 4.7. The coverage provided by the single cell DAS is limited to small and medium size buildings because of the antenna line losses and capacity of single cell [34]. Thus, coverage inside the large buildings can be improved using multiple cell strategy.

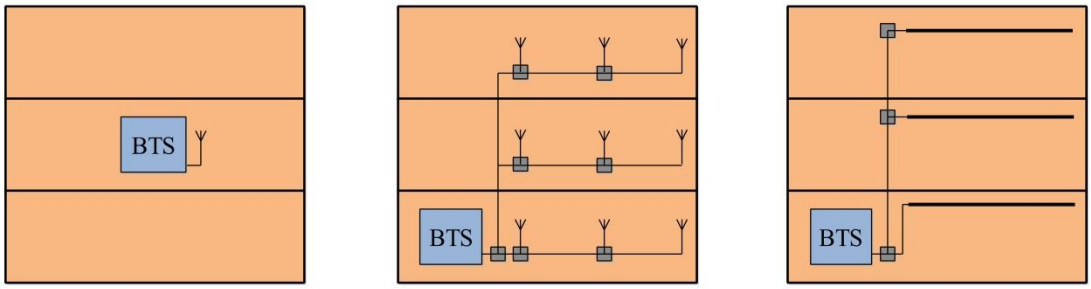

(a) (b) (c)

Figure 4.7. *Single cell strategy. (a) Small indoor cell (b) DAS (c) Radiating cable [34].*

In Figure 4.7, the square box with tangerine colour represents the single building with three floors. As shown in Figure 4.7 (a), a single small cell is implemented to cover the whole building. Furthermore, indoor coverage from a single cell can be improved by using DAS and radiating cable in each floor as shown in Figure 4.7 (b) and 4.7 (c) respectively.

4.5.6. Multi-cell Strategy

In multi-cell strategy, more than one indoor BTS are used inside one building to form multiple cells. These multiple cells improve the coverage inside the building, but the capacity improvement depends on the proper planning. Since there are multiple cells inside the same building, the risk of inter-cell interference increases which may deteriorate the capacity of system [34]. Hence, while planning multi-cell strategy, sufficient handover zones should be created to insure coherent coverage if there is any cell over lapping. Cell over lapping should be minimized as far as possible to reduce interference. Figure 4.8 shows the multi-cell strategy together with DAS and radiating cable implantation.

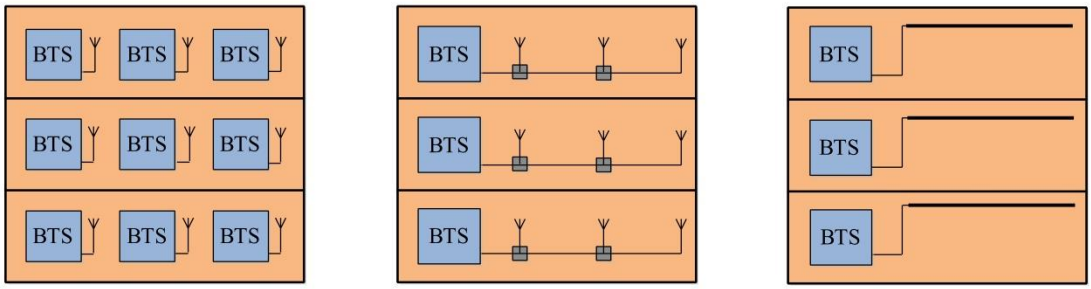

(a) (b) (c)

Figure 4.8. *Multiple cells strategy. (a) Small indoor cells (b) DAS (c) Radiating cables [34].*

5. FSS THEORY

FSS is the assembly of identical planar structures which behave as an EM filters [35-38]. FSS can also be defined as a metallic surface designed to be frequency selective in nature based on its reflecting/transmitting properties [36]. The smallest identical element of the FSS may contain one or more elements, and is known as unit cell. These unit cells are arranged periodically in one or two dimensional array to form the entire structure. Generally, the unit cell consists of conductive patch on a substrate or its complimentary geometry having aperture element of different shapes in a conductive surface [37]. The incident plane wave on FSS either gets reflected or transmitted around its resonance frequency. FSSs comprised of conductive patches reflect nearly all the incident EM waves at the resonant frequency whereas aperture transmits almost all the EM waves at resonance [37]. Thus, FSS can be designed as high pass, low pass, band stop, and band pass filters as shown in Figure 5.1. The characteristics of the EM filter mainly depend on FSS's element type and shape.

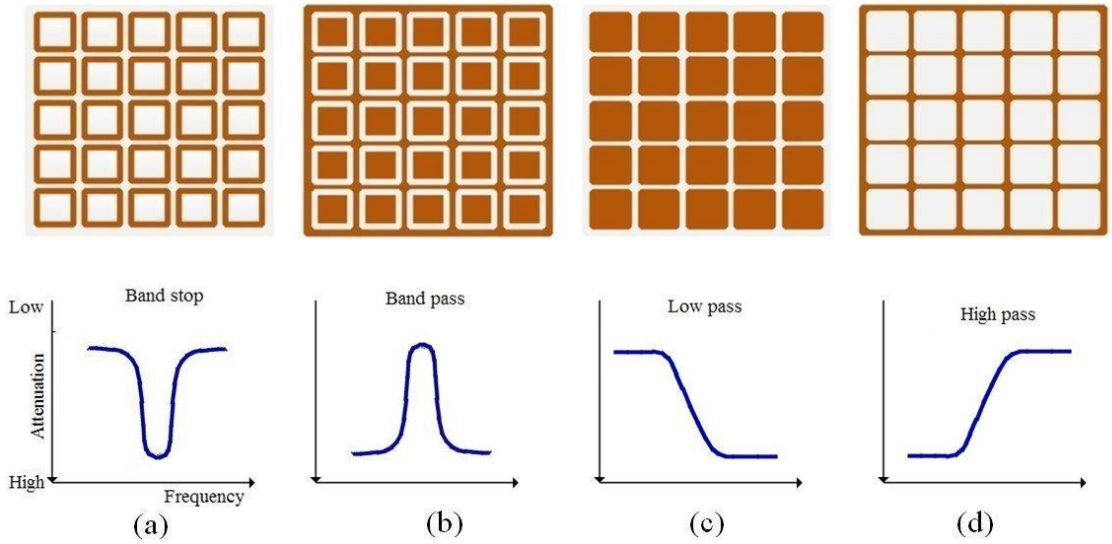

Figure 5.1. *Four types of EM filters; (a) Band stop (b)Band pass (c)Low pass (d) High pass [35]. Brown color represents conductive part.*

Let us choose the dipole element for theoretical analysis purpose since it is the basis for most of the other element types. Suppose dipole elements are arranged in two-dimensional infinite array with element length $2l$ and inter-element spacing D_x and D_z as shown in Figure 5.2. Dipole element will resonant when its length is equal to half of the wavelength of the incident wave. Each dipole is loaded at its center with load impedance Z_L. Such array can be categorized into passive and active array depending on the excitation method. For passive array, the structure is excited by an incident plane wave

$\boldsymbol{E}_i$ as shown in Figure 5.2 (a) and for active array the structure is excited by individual generators (V_g) connected to each element as shown in Figure 5.2 (b) [39].

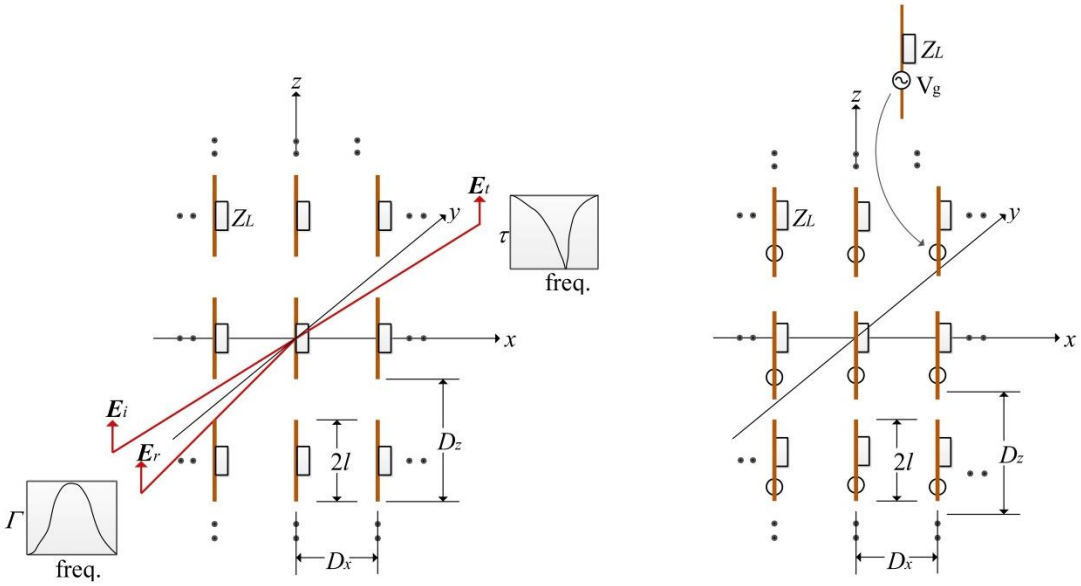

(a) (b)

Figure 5.2. *FSS with dipole as unit cell. (a) Passive array (b) Active array [39].*

For active array, each voltage generator must have the same amplitude and linear phase variation for it to works as FSS. But in case of passive array, the incident plane wave ($\boldsymbol{E}_i$) will be partly reflected back ($\boldsymbol{E}_r$) and partly transmitted in the forward direction ($\boldsymbol{E}_t$). At resonant condition, if E_i, E_r and E_t are the amplitudes of incident, reflected and transmitted plane wave respectively, then the reflection coefficient (Γ) and the transmission coefficient (τ) can be defined as

$$\Gamma = \frac{E_r}{E_i}, \tag{5.1}$$

$$\tau = \frac{E_t}{E_i}. \tag{5.2}$$

Since active arrays are difficult to realize as FSS in practice, only passive arrays are considered as FSS hereafter.

5.1. Complementary Arrays

Let us consider the arrays of slots with load admittance Y_L as shown in Figure 5.3. Such array can also be excited passively or actively as discussed above. The main difference between array of dipoles in Figure 5.2 and array of slots in Figure 5.3 is that the electric currents on the wires of dipoles are excited in dipole case while magnetic currents in slot case (that is, there is a voltage distribution in the slots). Magnetic currents are imaginary; that is, they do not exist. However, the electric field present in the slots can be shown equivalent to a magnetic current density by equivalence principle. The magnetic

current approach leads to a very desirable symmetry relationship between the dipole and slot cases. [38.] The electric field in the dipole case and magnetic field in the slot case are quite similar and symmetric [39]. The plots of the reflection and transmission coefficient with frequency are also shown in Figure 5.3. The reflection coefficient plot shows the total reflection of the incident wave whereas transmission coefficient plot shows the total reflection at certain frequency.

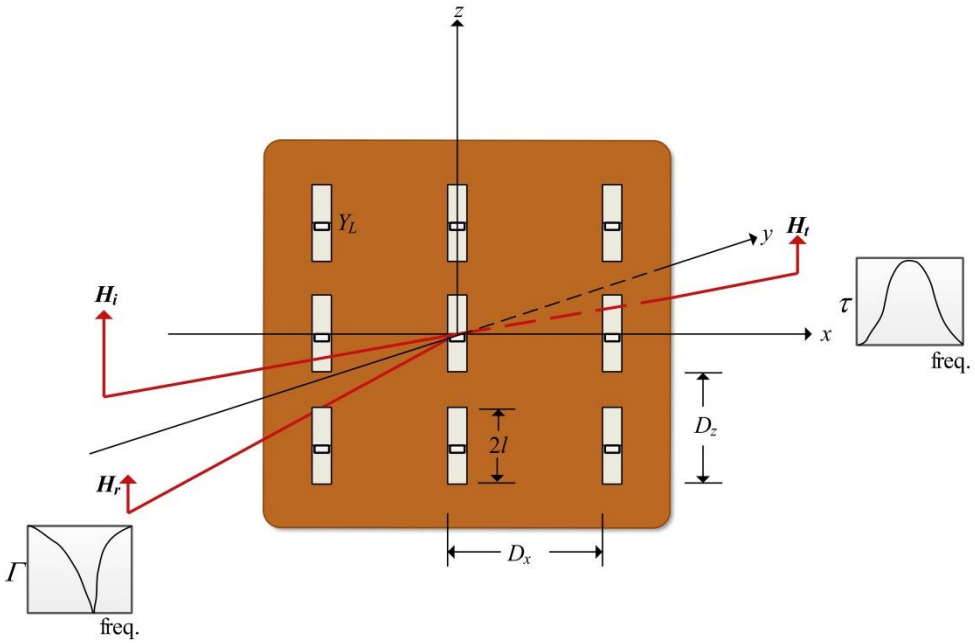

Figure 5.3. *Array of slots [39].*

Complementary arrays can be defined as an array of opaque and slot elements of similar shape such that if one is placed on top of other forms a complete perfectly conductive plane object. In optics, Babinet's principle for complementary screens states that '*the sum of the wave transmitted through a screen, plus the wave transmitted through the complementary screen, is the same as if no screens were present*' [40]. As according to Babinet's principle for complementary arrays, in electromagnetic fields the transmission property of one array is similar to reflection property of other array [35; 39; 40].

The reflection coefficient (Γ) of dipole array in Figure 5.4 (a) is equal to the transmission coefficient (τ) of slot array in Figure 5.4 (b) as long as the conducting screen is a Perfect Electric Conductor (PEC) and infinitely thin (typically less than 1/1000 of wavelength of the incident wave) in the absence of dielectric substrate [36; 39; 41]. Hence slot element is Babinet complement of dipole element. The consequences of thicker screen and dielectric are discussed in section 5.3.3 and section 5.3.4 respectively.

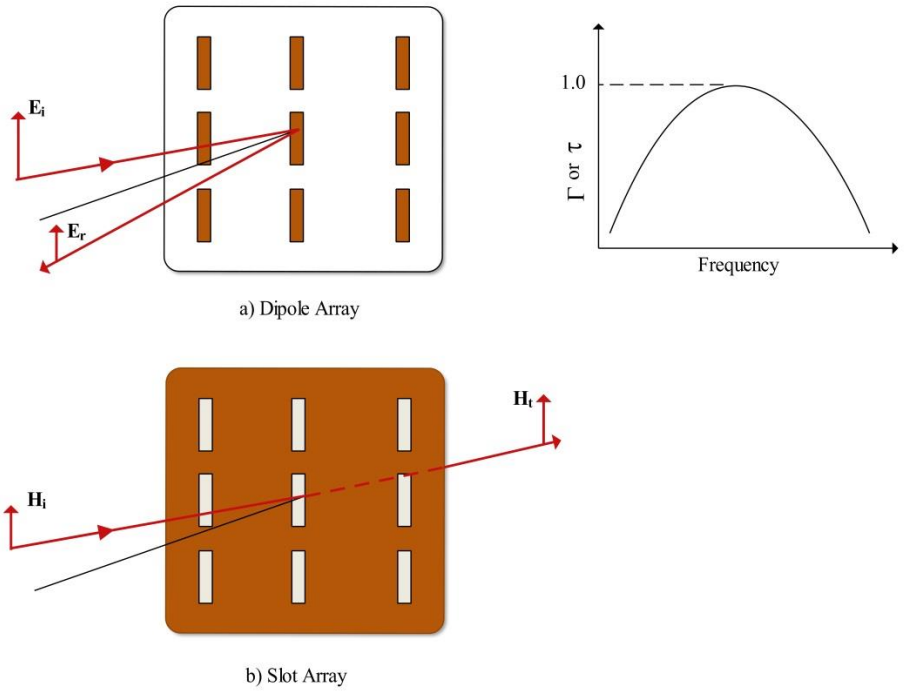

Figure 5.4. *Complementary Array (example of Babinet's principle) [39].*

5.2. Propagation of Waves in a Periodic Structure

The solution of the EM waves, in a periodic structure, is usually derived using Floquet's theorem [42]. Considering a periodic structure which has an infinite number of periods, Floquet's theorem states that '*for a given mode of propagation at a given steady-state frequency the electric or magnetic fields at one cross-section differ from those a period away only by a complex constant*' [37; 38; 42]. For simplicity, let us consider one-dimensional periodic structure along *x*-direction with uniform period p_x. From floquet's theorem, the EM fields $\boldsymbol{U}(x,y,z)$ for such structure satisfies the following equation,

$$\boldsymbol{U}(x + p_x, y, z) = \boldsymbol{U}(x, y, z)e^{-jk_{x0}p_x}, \tag{5.3}$$

Where $k_{x0} = \beta_{x0} - j\alpha_x$ is a complex wavenumber (fundamental propagation constant) that describes the phase shift (β) and the attenuation (α) of the field between different cells of the periodic structure. Consequently the field in the structure can also be described as

$$\boldsymbol{U}(x, y, z) = \boldsymbol{P}(x, y, z)e^{-jk_{x0}x}, \tag{5.4}$$

where $\boldsymbol{P}$ is a periodic vector function such that

$$\boldsymbol{P}(x \pm mp_x, y, z) = \boldsymbol{P}(x, y, z), \tag{5.5}$$

and *m* is an integer. Since the vector function $\boldsymbol{P}$ is periodic, it can be represented in a Fourier series as,

$$\boldsymbol{P}(x,y,z) = \sum_{m=-\infty}^{+\infty} \boldsymbol{A}_m(y,z)\, e^{-j\left(\frac{2\pi m}{p_x}\right)x}, \tag{5.6}$$

where $\boldsymbol{A}_m$ is the coefficient of $\boldsymbol{P}$. Substituting equation (5.6) in equation (5.4), the general expression of wave in periodic structure can be obtained as:

$$\boldsymbol{U}(x,y,z) = \sum_{m=-\infty}^{+\infty} \boldsymbol{A}_m(y,z)\, e^{-jk_{xm}x}, \tag{5.7}$$

where

$$k_{xm} = k_{x0} + \frac{2\pi m}{p_x} = \left(\beta_{x0} + \frac{2\pi m}{p_x}\right) - j\alpha_x = \beta_{xm} - j\alpha_x. \tag{5.8}$$

Hence, the EM field $\boldsymbol{U}$ can be expressed as a sum of an infinite number of travelling waves of the form $\boldsymbol{A}_m(y,z)e^{-jk_{xm}x}$, called Floquet harmonics [36]. Since FSS is also a periodic structure, it is sufficient to describe the field in terms of only one unit periodic cell.

5.3. Design Parameters for FSS

The factors which determine the performance of the FSS can be summarized into four main parts, which are: FSS's element geometry; FSS's element conductivity; substrate which supports the FSS and the incidence angles of incoming signals.

5.3.1. Periodic Array Spacing

The distance between any two periodic cells (or unit cells) is known as periodic array spacing. The array spacing is the function of operating frequency. While designing the FSS, array spacing should be chosen such that granting lobes phenomenon does not occur. Granting lobes are the undesired secondary beams that appears when the array spacing is electrically large compared to the wavelength (λ) of operating frequency as shown in Figure 5.5 [35]. These secondary beams reduce the energy in the main transmitted or reflected beam [37]. In order to prevent granting lobes to occur, the element size and array spacing should be kept less than one wavelength at 0° incidence angle [35].

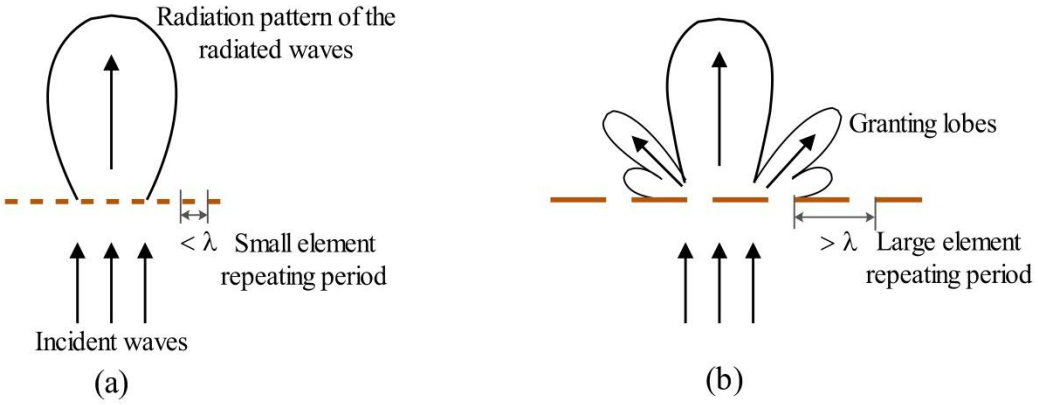

Figure 5.5. *Granting lobe phenomenon. (a) Single main beam without granting lobes. (b) Granting lobes occur with multiple propagation modes excited [35].*

5.3.2. Element Types (or Geometry)

The performance of the FSS is heavily dependent on its element shape and the following characteristics are affected by it [37].

- Angular stability
- Bandwidth
- Band Separation
- Cross-polarization levels

Angular stability defines the sensitive of element shape towards the varying incident angels. Frequency transition from pass bands to stop bands or separation of transmission and reflection center frequencies accounts for band separation. Cross-polarization level gives the inconsistency of frequency response between different polarized wave (like TE and TM incident wave). Cross-polarization is the radiation perpendicular to the desired polarization.

The element shapes of FSS can be chosen arbitrary, but as presented by Munk in [39], it can also be classified into following four groups:

5.3.2.1 Center Connected or N-poles

This group consists of element shapes such as dipoles, tri-poles, and Jerusalem crosses. The centre connected FSS element will resonate if the leg of the element is about half of a wavelength [37]. FSS like dipole elements can only handle linear polarization with the electric field being in the plane of element. But it can handle all polarization if combined with two elements twisted 90 degrees with each other like cross-dipole [39].

Figure 5.6. *Center connected or N-Poles [39].*

5.3.2.2 Loop Types

Element shapes such as square, circular and hexagonal loops belong to this group. Typically for loop element resonance will occur if the total element length is approximately equal to one wavelength [36]. Thus, the element size is smaller than a quarter of a wavelength. These types of FSS are commonly used because of its wide range of bandwidth.

Figure 5.7. *Loop Types [39].*

5.3.2.3 Solid Interior or Plate Types

This group consists of various shapes such as squares, circles, rectangles and hexagons. These types of elements were the first to be investigated. The dimension for these types of elements is closely half wavelength.

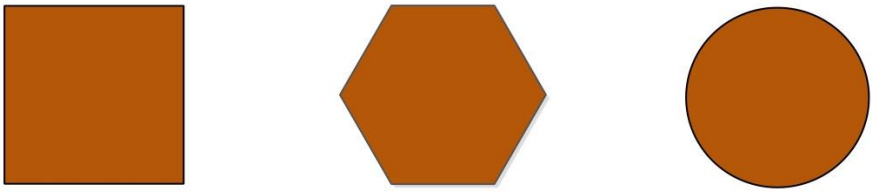

Figure 5.8. *Solid Interior or Plate Type [39].*

5.3.2.4 Combination

In this group, element shape consists of the combination of any of the above describe element shapes. So it may have endless combinations and variation of elements. However, it is difficult to make the initial guess of the resonance frequency for solid interior (plate) type and combinations.

Figure 5.9. *Combinations [39].*

5.3.3. Conductivity and Thickness of FSS Layer

Conductivity here refers to the electrical conductivity of the material used to form FSS. Electrical conductivity is defined as a measure of material's ability to conduct an electric current through them. When an electromagnetic wave hits the FSS, currents are induced on the conducting elements of FSS. This induced current again radiates EM waves from the conducting elements similar to that of conductive posts or strips inside a rectangular waveguide [45]. However, if the material conductivity degrades or becomes lossy, the incident wave power dissipated as heat in the element. As a result, the overall performance of FSS degrades. For example, the transmission of the incident wave through a slot (or aperture) array at the resonant frequency reduces with decreasing material conductivity until it loses its frequency selective nature.

Thickness of FSS layer has an effect on its bandwidth [39]. Bandwidth can be defined as the frequency response of the system that lies within -3dB of the response at its peak. If the maximum gain of the system is 0 dB, the -3 dB bandwidth is the range of frequency where the gain is more than -3 dB. Depending on the wavelength (λ) of frequency, FSS can be divided into 'thick' or 'thin' layer. If the thickness of the FSS layer is less than 0.001λ, it is considered as thin or infinitely thin otherwise as thick. If the FSS layer becomes thicker, the bandwidth of aperture array will be narrower [39] whereas for dipole array the bandwidth will be wider [39]. It is a well-known fact, from antenna theory, that the bandwidth of a dipole antenna generally increases with wire radius.

5.3.4. Dielectric Substrate

Dielectric substrates are often used to provide supporting structures mainly for mechanical reasons. Adding a dielectric slab around a FSS not only changes its resonant frequency significantly but also stabilizes the angular response [35; 39; 46]. Dielectric substrate can either be added to one or both sides on FSS. If an infinite dielectric material with relative dielectric constant (ε_r) is added to the both sides of FSS, the resonant frequency will reduce by the factor $\sqrt{\varepsilon_r}$ as seen from Maxwell's equations [39].

The effect of infinite dielectric material to FSS's resonant frequency is illustrated in Figure 5.10 (a). If the dielectric material added on both sides of the FSS, is of finite thickness $2d$ as shown in Figure 5.10 (b), the change of resonant frequency will be in-between f_0 and $f_0/\sqrt{\varepsilon_r}$, where f_0 is the resonant frequency of free standing FSS. Even

if the dielectric thickness is as small as d ~ 0.05λ_ϵ (λ_ϵ − electrical wavelength), the resonant frequency is nearly close to $f_0/\sqrt{\varepsilon_r}$. When the dielectric substrate is present only on one side of the FSS as shown in Figure 5.10 (c), the resonant frequency reduced by a factor $\sqrt{(\varepsilon_r + 1)/2}$. For both dipole and slot array, the resonant frequency will shift downward with the addition of dielectric material. However, for dielectric thickness of $\lambda_\epsilon/4$ or more, these two types of array behave differently. The resonant frequency of dipole array is independent of dielectric thickness whereas slot array shows unit transmission at frequencies around$f_0/\sqrt{\varepsilon_r}$.

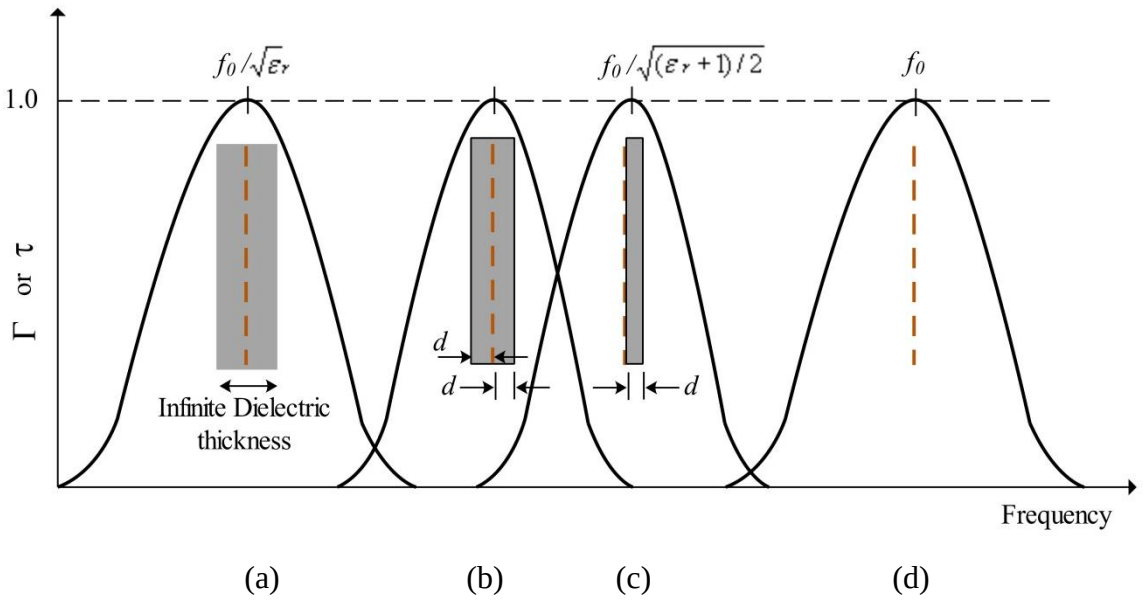

Figure 5.10. *Effect of dielectric on resonant frequency. (a) Infinite thick dielectric on both sides of FSS. (b) Dielectric of finite thickness d on both sides of FSS. (c) Dielectric of finite thickness d on one side of FSS. (d) Free standing FSS (without dielectric). Dotted brown line represents FSS. Typically d < ~ 0.005$\boldsymbol{\lambda_\epsilon}$ [39].*

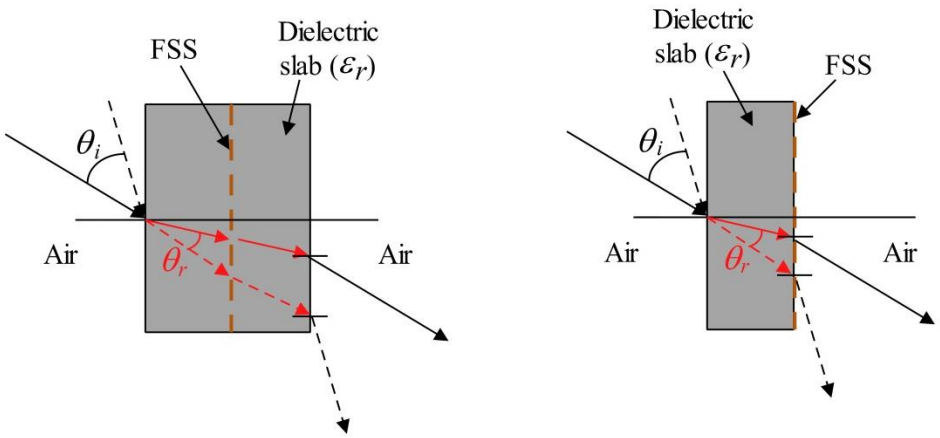

Figure 5.11. *Effect of dielectric on incident angle [35].*

Angular stability of FSS is a plus point of adding dielectric substrate to FSS. The angle of incident wave can be made stable to FSS by using the dielectric slab. According to Snell's law of refraction, the angle of refraction inside a dielectric slab is less than the angle of incident in free space (i.e.$\theta_r < \theta_i$) as shown in Figure 5.11. Hence, the range of incident angle to FSS inside the dielectric slab is reduced, making it more stable towards variation of incident angle [35].

5.3.5. Performance Analysis of Various Element Shapes

Each element shape of FSS presented in section 5.3.1 possesses its own unique frequency characteristics. The performance analysis of different free standing thin FSS element shapes is presented in Table 3.1 [11; see 35]. Performance of different element shapes is rated according to its four frequency characteristics: angular stability, cross-polarization level, bandwidth, and smallest band separation.

Table 5.1. *Performance analysis of FSS's different element shapes. [11; see 35]*

Element Shapes	Angular Stability	Cross-polarization level	Larger Bandwidth	Small Band Separation
Dipole	4	1	4	1
Jerusalem Cross	2	3	2	2
Rings	1	2	1	1
Tripole	3	3	3	2
Cross Dipole	3	3	3	3
Square Loop	1	1	1	1

Rating: 1-best, 2-second best…

As seen from Table 3.1, freestanding dipole element has the worst stability with incident angle variation. Hence, it also has the smallest operable bandwidth. The performance of the square loop element is rated best in all four characteristics compared to other element shapes as presented in Table 3.1.

5.4. Application of FSS

A typical application of FSS is in antenna radomes or electromagnetic shielding. A radome is a structure enclosing the antennas which is transparent to the operating frequency and opaque to the signals outside the operating band. Thus, depending on the radome's shape the signals outside the operating band can be reflected in different directions to reduce the backscattering radar cross section of an antenna. [39]. Therefore, FSS radomes are widely used for military purpose on missiles, aircraft or submarine.

One perfect example of electromagnetic shielding in daily life is microwave-oven. A microwave-oven has a circular hole metal door. It acts as a high pass filter which blocks the microwave frequency and allows visible light to pass through to monitor the cooking progress. Hence the oven door is optically transparent and at the same time acts like a closed metal shield to internal microwave transmission.

Another important application of FSS is sub-reflector in the Cassegrain system also known as dichroic structure. Such structure is transparent to one frequency band and opaque to another frequency band. This enables two distinct focal points accommodating two feed operating at two different frequencies under same main reflector.

FSS can also be used as circuit absorbers, polarizers and beam splitters. If the FSS possess polarization dependent resonance characteristic, such feature can be used to produce a polarizer. Meanderline polarizers are used to change the polarization of the wave, that is from linear to circular or vice-versa [39].If this polarization dependence is utilized such as to allow transmission of particular polarization while reflecting waves of other polarization, then such FSS can be used as beam splitter. In recent years, FSS finds its application in wireless communication systems too. FSS is used in the walls of the buildings like theatres, hospitals, prison cells or public libraries for blocking the mobile phone signals and allowing only emergency calls. Another use of FSS in modern communication system is the frequency selective windows as shown in Figure 5.12. Using a thin layer of metal in the window has become popular nowadays due to its thermal isolation property. This metallic coating blocks the heating radiation to increase the energy efficiency of windows. Such windows are commonly known as energy efficient windows or low-emissivity windows and are transparent to the visible part of the EM spectrum.

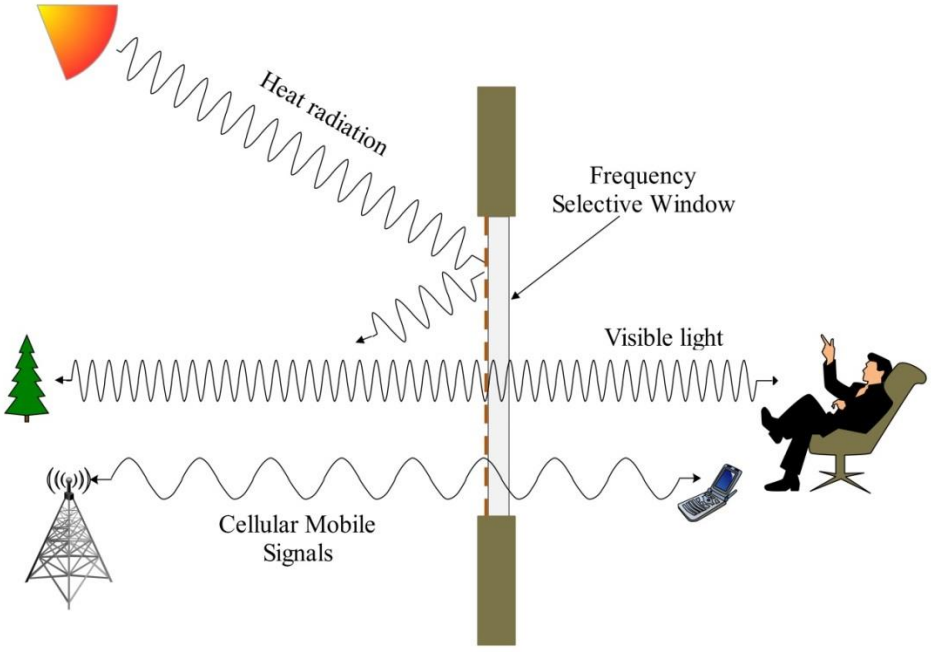

Figure 5.12. *Illustration of frequency selective window.*

Figure 5.12 demonstrates the functionality of frequency selective window. The infrared (or thermal) radiation is blocked by the window, but it is transparent to visible light and cellular radio frequencies. The free space wavelength of thermal radiation is 1 mm to 750 nm, of visible light is 380 nm to 780 nm, and of radio wave ranges from thousands of kilometres down to 0.1 mm [30]. These types of windows in modern houses are very problematic since they do not allow the propagation of radio waves through them. Hence it creates the indoor coverage issue. The solution to this problem is to develop the frequency selective windows which are capable of allowing radio waves propagation preserving its energy efficient nature. This is a new technique of improving indoor coverage in modern houses without additional network configuration. Basically, frequency selective windows are produced by creating FSS structures in the metallic coating of energy efficient windows. Research [8; 9; 38; 44; 50; 51; 52] has been carried out in this field of frequency selective windows for the efficient propagation of radio waves. However, the commercial production of the frequency selective windows has not known yet. The research in this field is still going-on.

6. FSS MODELLING AND SIMULATION

This chapter gives the brief description of the simulation software used for the modelling of FSS. It also explains the procedure of modelling the FSS along with each simulation step. Finally, the simulation results are presented with a short description.

6.1. Simulation Software

Computer Simulation Technology (CST) Microwave Studio@ 2012 [47] was used to model and simulate the FSS. It is a high performance electromagnetic simulation software for fast and accurate analysis of high frequency applications. It is a full three-dimensional EM wave solver based on Finite Integration Technique (FIT) which is the integral form of Maxwell's equations. FIT allows the problem to be solved on a Cartesian (Hexahedral) or general non-orthogonal (Tetrahedral) grids both in the time domain as well as the frequency domain. [48]. In this thesis, frequency domain solver using tetrahedral mesh with full Floquet modal expansion and periodic boundaries was used to calculated the resonant frequency of the unit cell. More about FIT can be found on [48].

Angular stability is an important feature of FSS. In a real case scenario, the angle of incidence wave is arbitrary. Therefore, the FSS should exhibit similar characteristics for varying angle of incidence. In CST MW studio software, the incidence angle of the incoming plane wave can be controlled by varying angles theta (θ) and phi (Φ) as shown in Figure 6.1 (a). Two Floquet modes (TE and TM) were set in the simulator for ports Zmin and Zmax. For off-normal incident angles, the Floquet port modes ensure that the reflected wave is recorded in the direction of optical reflection while the transmission is in the same direction as the incident wave as illustrated in Figure 6.1 (b).

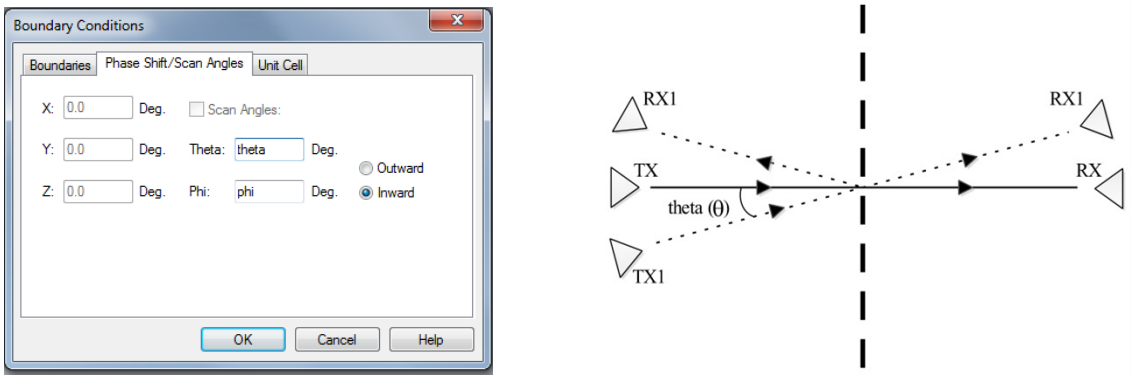

(a) (b)

Figure 6.1. *Incident plane wave angle setting.*

6.2. Unit Cell Approach

CST Microwave Studio makes the analysis of periodic FSS structures much easier with its in-built template: FSS-unit cell. Only one constituting element of the FSS array is analysed with the help of Periodic Boundary Condition (PBC) together with Floquet's theorem as if there were infinite periodic elements. This constituting element is referred as unit cell, and the periodic boundary condition is known as unit-cell boundary. In unit-cell simulation, radiation boundaries are applied to the back and front end while unit-cell boundaries to all other four sides of unit-cell. Unit-cell of FSS is illuminated with a plane wave at the front end. The minimum and maximum of *x*- and *y*-directions are set to a unit cell, whereas z-directions were set to open (add space). Thus, the transmission coefficient is computed through the unit-cell rather than the whole array.

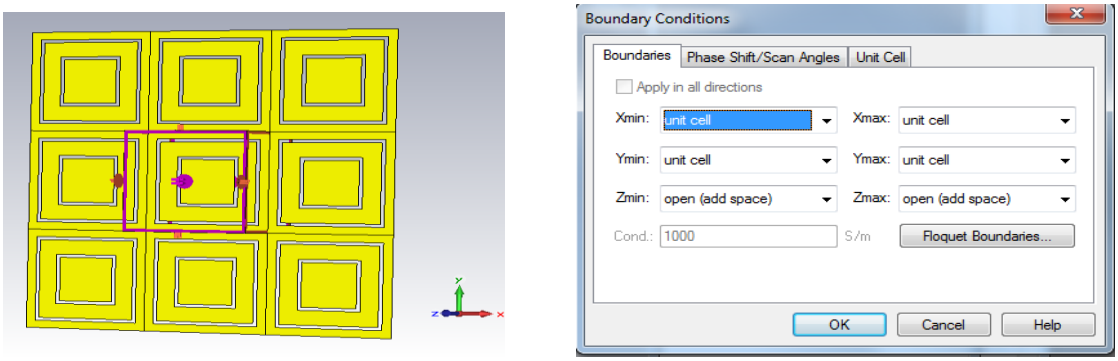

Figure 6.2. *Unit-cell boundary conditions.*

Figure 6.2 shows the unit-cell boundary conditions. The unit-cell boundaries are applied in *x*- and *y*-directions indicating the simulation results are for infinite array structure. Since only the unit-cell is analysed rather than the whole array, the simulation computational time is reduced significantly. This is the reason why unit-cell approach has been adopted.

6.3. FSS Model

Square loop element shape was chosen for the FSS analysis purpose, due to the structural simplicity and best suitable for all four frequency characteristics as discussed in section 5.3.5. In order to meet the objective of this thesis, the frequency selective characteristics of FSS should be double band-pass. Hence, each band is realized by a square loop aperture element. The dimension of the unit cell of double square loop aperture FSS is shown in shown in Figure 6.3. According to dimension of the unit cell shown in Figure 6.3, 15.48% of the conducting area is removed from the total area of unit cell.
The relation between the increase in thermal radiation transmission and the percentage of coating area removed by FSS elements is approximately linear [49; see 51]. Hence, approximately extra15% of thermal radiation will transfer through the FSS with the shown unit cell parameters.

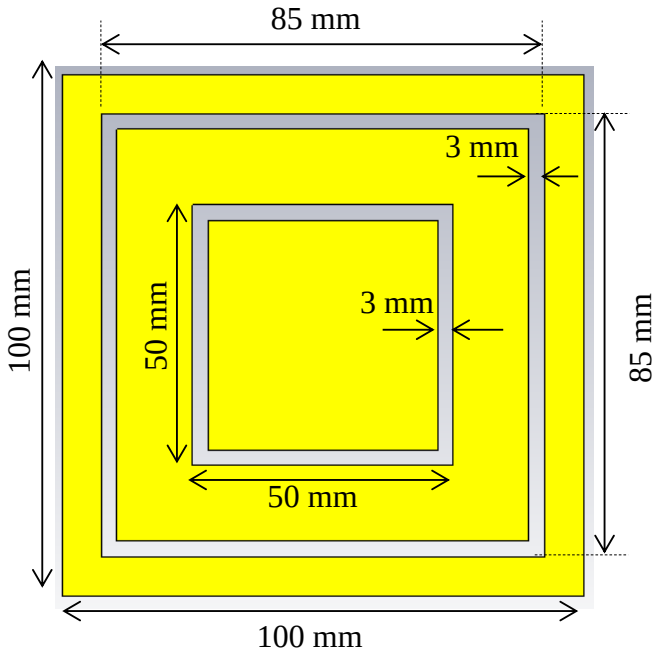

Figure 6.3. *Unit cell geometry.*

It is a freestanding FSS, meaning it has no dielectric material for support. For loop type FSS, resonance occurs when the total length of the loop is approximately one wavelength. The larger square loop aperture was tuned for GSM900 band and a smaller loop for GSM1800 and UMTS2100 band. Hence, a dual band-pass FSS structure was realized which had resonant frequency at 950 MHz and 1900MHz. The resonant frequency of 1900 MHz was chosen to cover both the GSM1800 and UMTS2100 frequency band. The conducting material of FSS was modelled using an aluminum metal in the simulator. A very thin layer of conducting material was realized by using an approximation of zero thickness. The characteristics of the aluminum used to model the conducting part of FSS consists of following parameters: relative permeability = 1, electric conductivity = 3.56×10^7 S/m, thermal conductivity = 237 W/K/m and material density = 2700 kg/m^3. In Figure 6.3, yellow part represents the conducting part, and two squares represent apertures of 3 mm size each.

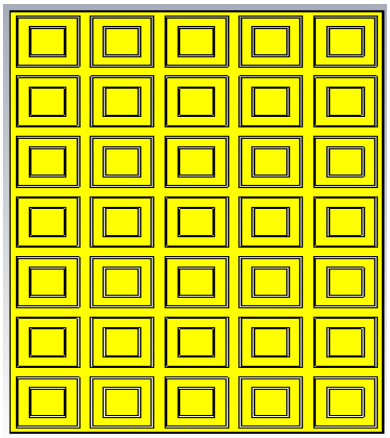

Figure 6.4. *5×7 unit cell geometry.*

The unit cell boundary performs simulation for an infinite array. Considering the fabrication part, infinite array is impossible to make, so a reasonable array was chosen. In this thesis, 5×7 array of the unit cell was chosen for analysis as shown in Figure 6.4. Hence the final dimension of FSS was 500×700 mm.

6.4. Simulation Results

Figure 6.5 shows the transmission curve of free standing Double Square loop FSS. It has dual band pass response with center frequency 950 MHz and 1900 MHz. The purpose of choosing the 1900 MHz as one center frequency is to cover both 1800 MHz and 2100 MHz frequency. In Figure 6.5, marker 1, 2, 3 and 4 shows the -3 dB point for first and second band pass region. The first reading of the each marker shows the frequency in MHz and the second reading shows transmission level in dB. Hence the -3 dB transmission bandwidth for first band-pass region with 950 MHz and second band-pass region with 1900MHz center frequency is 433 MHz and 632 MHz respectively. It covers both GSM and UMTS frequency bands.

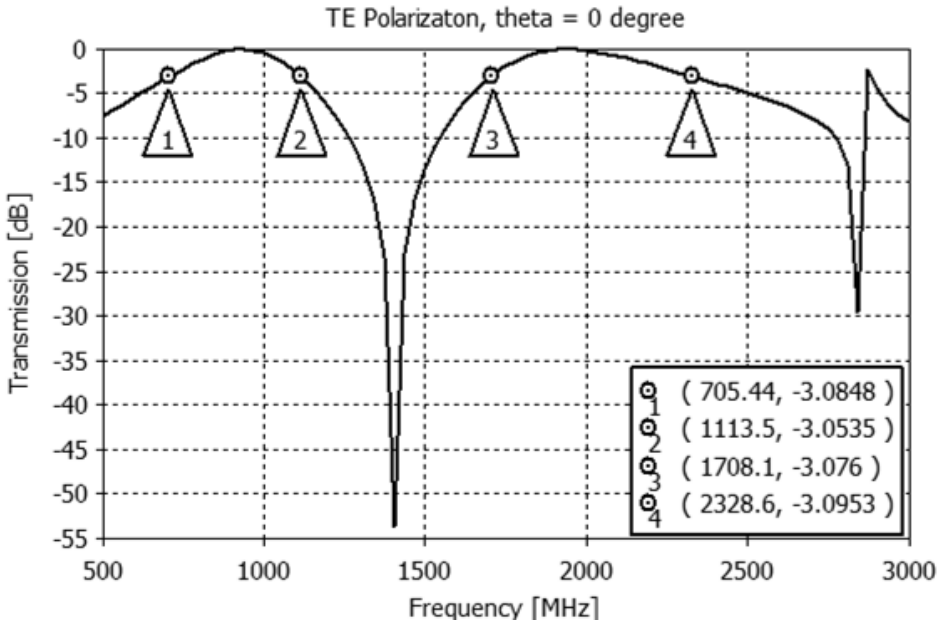

Figure 6.5. *Transmission curve at normal angle of incidence for free-standing FSS.*

Fig 6.6 shows the signal transmission through aluminum foil and FSS. For aluminum foil, the transmission loss is 200 dB which seems unrealistic. It is hard to believe such attenuation for real aluminum foil. Such result for unrealistic simulation result for aluminum foil may be because the simulator considers aluminum very similar to PEC.

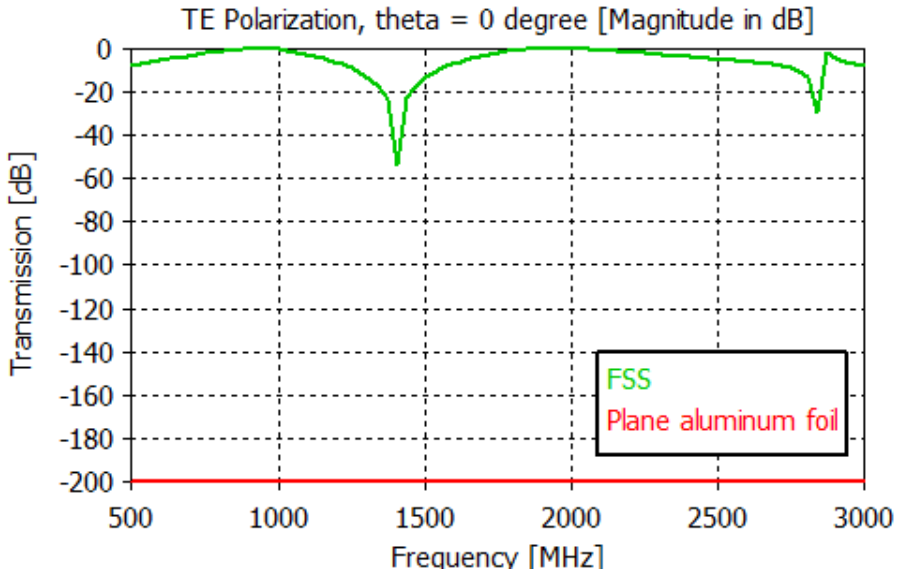

Figure 6.6. *Transmission curve comparison of free-standing FSS and foil at normal angel of incidence.*

TE and TM Mode

Figure 6.7 (a) shows the simulation result of free-standing FSS for TE polarization at varying incident angle. When the angle of incident increases from 0° to 40°, the resonant frequency of lower band-pass region remains constant, but at upper band-pass region, granting lobes start to increase. Also, the bandwidth is decreasing with increasing incident angle at upper band-pass region. It shows that the free standing FSS does not have angular stability at higher frequencies. Such angular instability of free standing FSS can be improved by the adding a dielectric substrate to the FSS. The simulation result for FSS with a dielectric substrate on one side is shown in Figure 6.7 (b).

The overall FSS response will be affected by the dielectric property of the substrate to which the FSS is attached as discussed in chapter 5, section 5.3.4. The relative permittivity (ε_r) of the dielectric substrate was assumed to be 2. The presence of a dielectric medium on one side of the FSS shifts the resonant frequency downwards by a factor $\sqrt{(\varepsilon_r + 1)/2}$, which is 1.22. At 0° incident angle, the freestanding FSS resonates at 950 MHz and 1900 MHz, and FSS with substrate resonates at 800 MHz and 1650 MHz. Figure 6.7 (b) also shows that the angular stability is improved by addition of the dielectric substrate compared to free-standing FSS. However, granting lobe starts to propagate only after 40° incident angle.

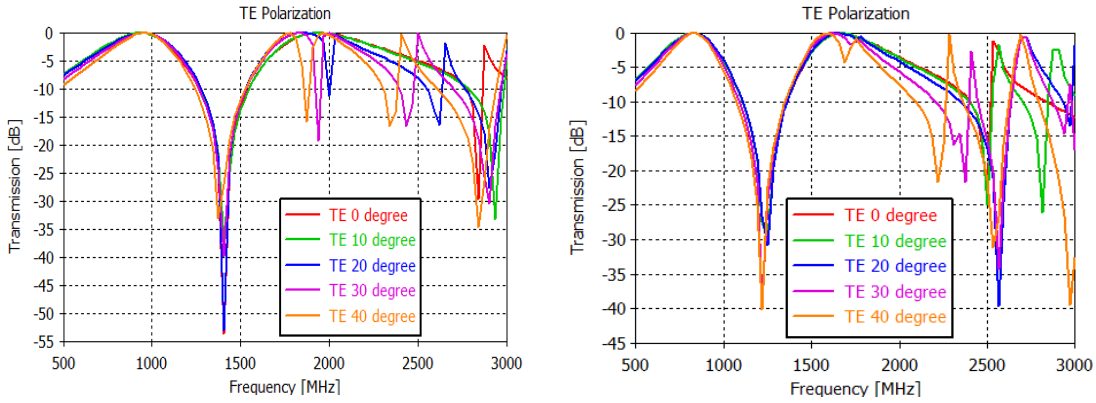

(a) *(b)*

Figure 6.7. *TE Polarization at varying angle of incidence. (a) Free-standing FSS (b) FSS with a dielectric substrate on one side.*

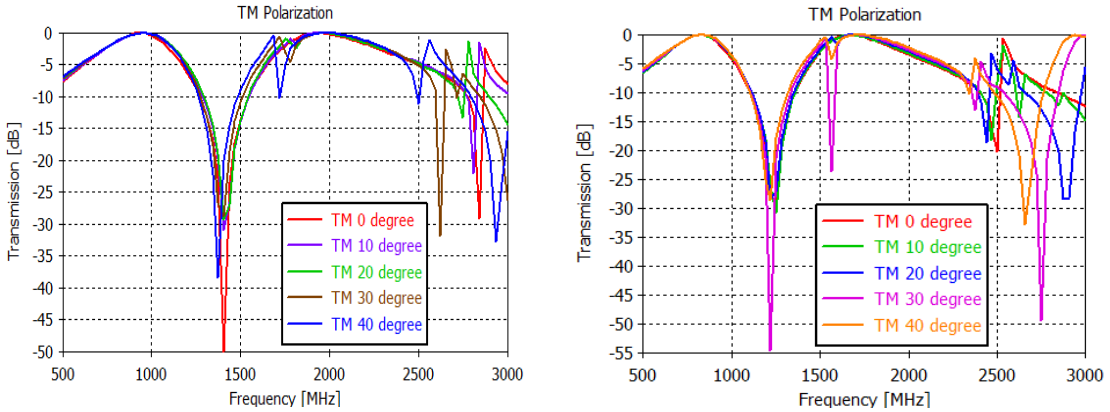

(a) *(b)*

Figure 6.8. *TM Polarization at varying angle of incidence. (a) Free-standing FSS (b) FSS with a dielectric substrate on one side.*

Figure 6.8 (a) and (b) shows the simulation results of free-standing FSS and FSS with dielectric for TM polarization respectively. For TM polarization, the resonant frequencies of lower and upper band-pass regions are consistent for different incident angle. The higher order modes around upper band-pass regions are pushed to a higher frequency as compared to TE polarization case. It shows TM polarization has more angular stability compared to TE polarization.

7. MEASUREMENTS AND ANALYSIS

Before starting the measurements, the FSS prototype was fabricated in the laboratory as according to the modelled dimension. The process of FSS fabrication along with measurement details are presented in this chapter.

7.1. FSS Fabrication

Double square loop aperture FSS prototype was constructed using aluminum foil. According to the dimension of the unit cell as specified in Figure 6.2, a large sheet of aluminum foil was hand-cut into an array of square elements. Each element was then pasted on a plastic board of 3 mm thickness as shown in Figure 7.1(a). Since a free-standing FSS is difficult to handle during fabrication and measurement process, plastic board was used for structural support. This plastic board is acting as a dielectric substrate on one side of FSS which has a significant effect on frequency characteristics as discussed in chapter 5, section 5.3.4. Finally, 5×7 array FSS prototype was fabricated as shown in Figure 7.1(b).

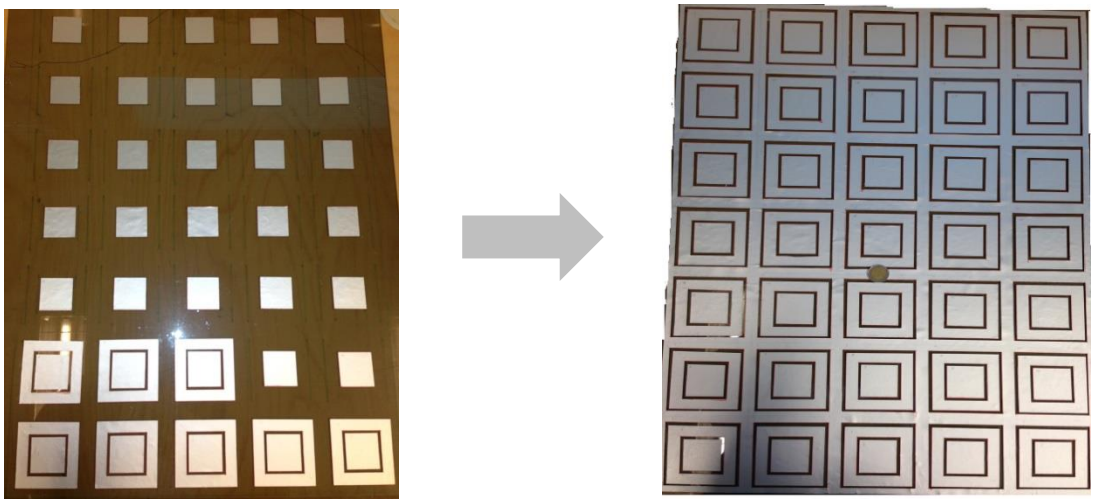

(a) *(b)*

Figure 7.1. *FSS prototype fabrication process. (a) Initial stage (b) Final stage*

7.2. Laboratory Measurement

The FSS prototype was measured in the laboratory of the Tampere University of Technology. This laboratory has two separate rooms partition with a wall having glass structure at the center. The FSS was measured on this glass window located on the wall. Remaining part of the wall was shielded with insulation board to ensure the signal propa-

gation only through FSS. Since the room is not an anechoic chamber, the signals propagate via diffraction, reflection or scattering, to reach the receiver antenna. Hence, the received signal contains strong line of sight components as well as multipath components. Such multipath signal propagation leads to the oscillatory transmission curves with unwanted ripple levels. Such ripples were handled while post-processing the measured data in the Matlab.

7.2.1. Measurement Setup

Two identical horn antennas (A-INFO JXTXLB-880-NF) were used for measurement purpose; one as a transmitting antenna (TX) and other as a receiving antenna (RX). Transmitting antenna was connected to a signal generator (Rohde&Schwarz SMJ100A) and receiving antenna to a spectrum analyzer (Rohde&Schwarz FSG) via RF cables (RG213). Both antennas were at same height, which is 1.78 m. To ensure the measurements in the far field zone, two antennas were kept around 4 m apart. The distance of FSS from TX and RX antenna are 2 m respectively, and both antennas were aligned in line of sight. The overall measurement setup is shown in Figure 7.2.

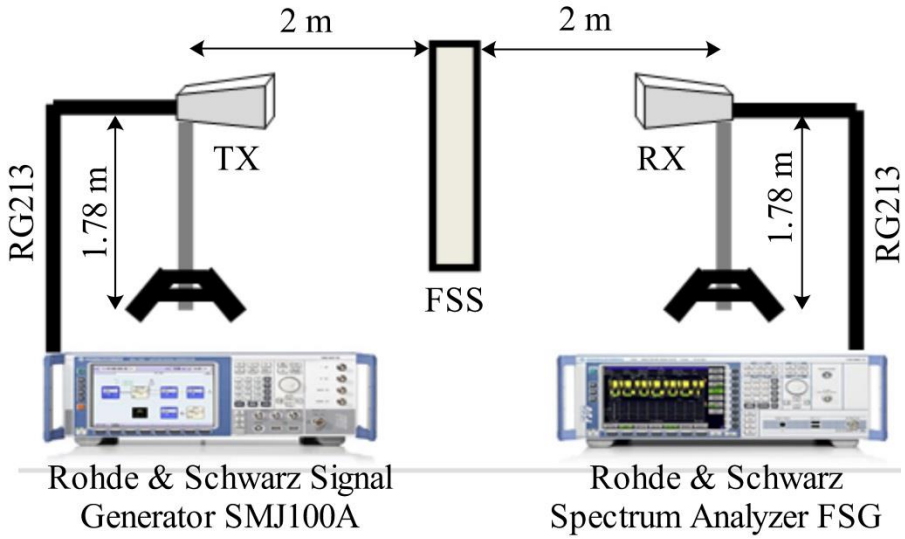

Figure 7.2. *Measurement setup [4].*

To observe the effect of FSS in RF signal transmission, three measurements were made with the following setups.

- Signal propagation through the aperture of FSS size as shown in Figure 7.3 (a). This is the free-space propagation measurement and is taken as a reference for normalizing.
- Signal propagation through aluminum foil as shown in Figure 7.3 (b).
- Signal propagation through FSS as shown in Figure 7.3 (c). Different incident angle measurement were measured by varying angle theta (θ) from 0° to 10°, 20°, 30°, and 40° as shown in Figure 7.3 (d).

Finally, the signal transmission through aluminum foil and FSS were calculated by subtracting reference measurement data from the respective measured data to normalize the measurement results.

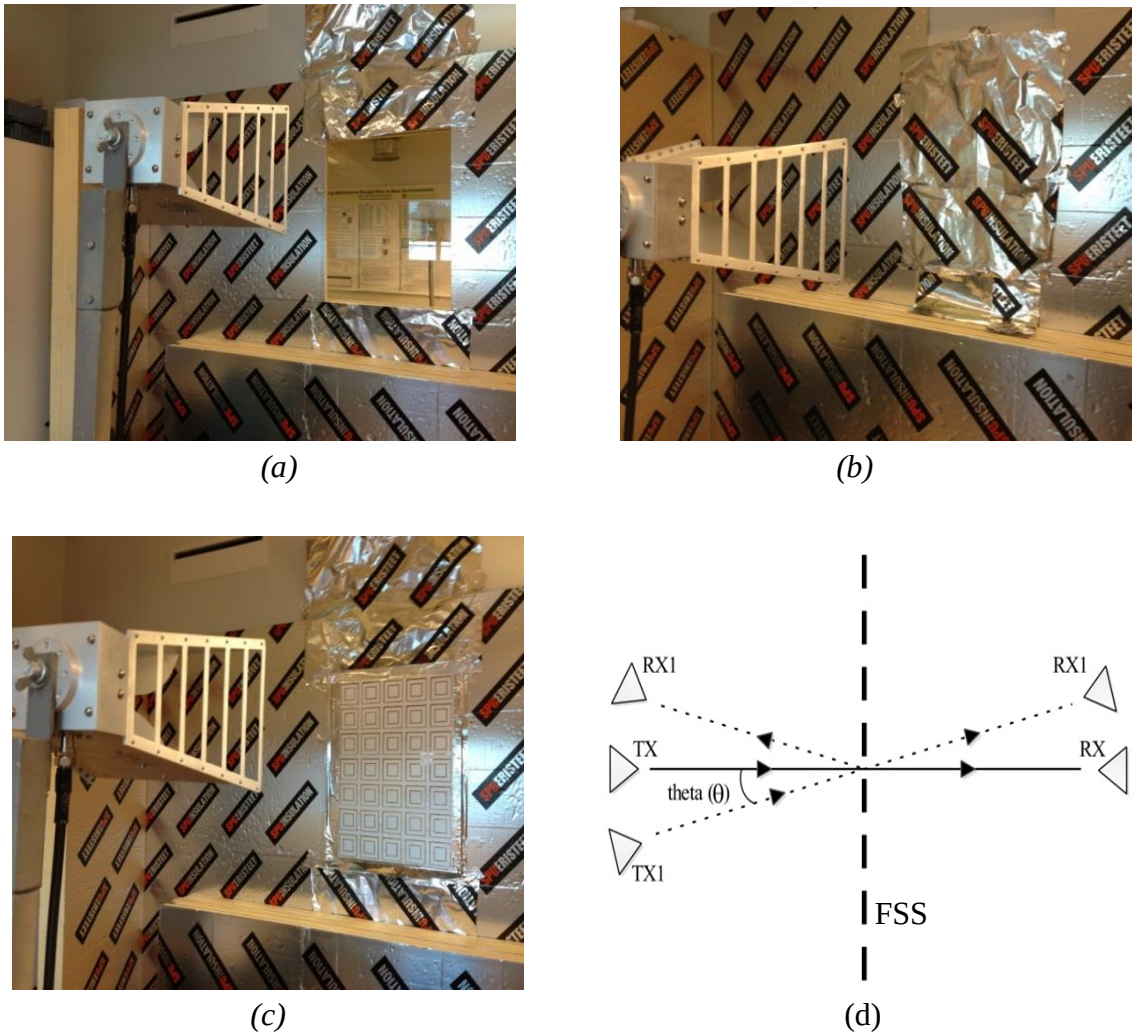

Figure 7.3. *Measurement setup for (a) FSS size aperture (Reference), (b) aluminum foil (c) FSS prototype and (d) varying incident angle (θ).*

7.2.2. Lab Measurement Results

The range of frequency for the measurements was fixed from 500 MHz to 3000 MHz with a 50 MHz resolution. The RF signal power through the TX antenna was set to 0 dBm. The transmitted signal is received by RX antenna and collected with the help of a spectrum analyzer. The collected measurement data were then processed in Matlab. Due to the discrete and fluctuating nature of the measured data, data smoothing technique is applied to produce a smoothed trend line for easy comparison. Data smoothing tool in Matlab called LOESS (locally weighted scatterplot smoothing) is used, which use locally weighted linear regression to produce a smooth trend line. Raw measured data and

normalized data for TE and TM wave along with the smoothed trend lines are shown in Figure 7.4 and 7.5 respectively.

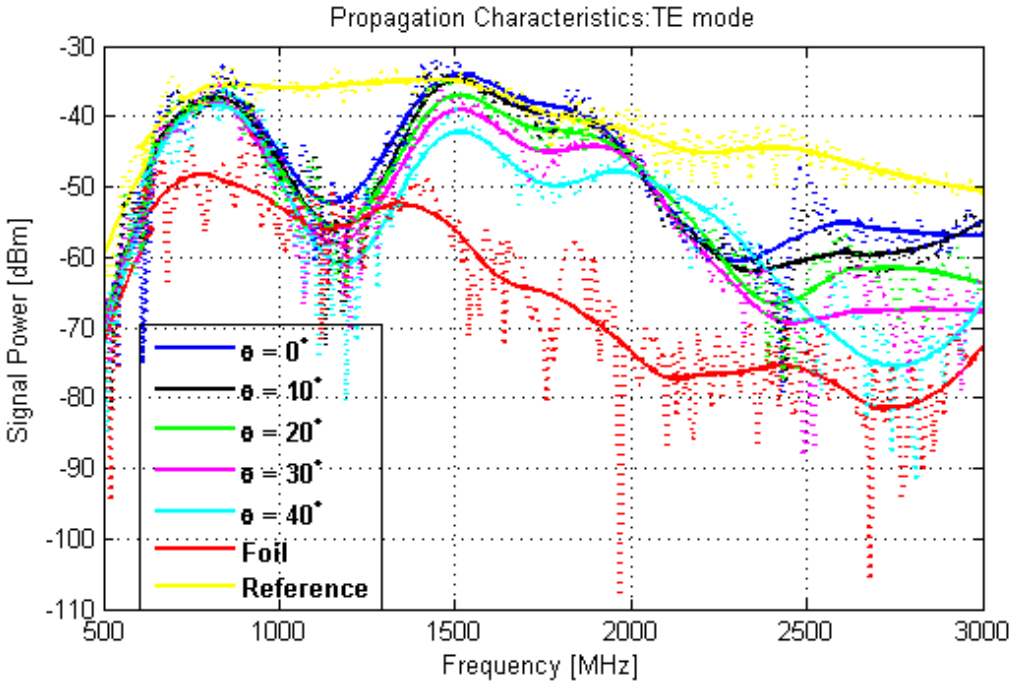

(a)

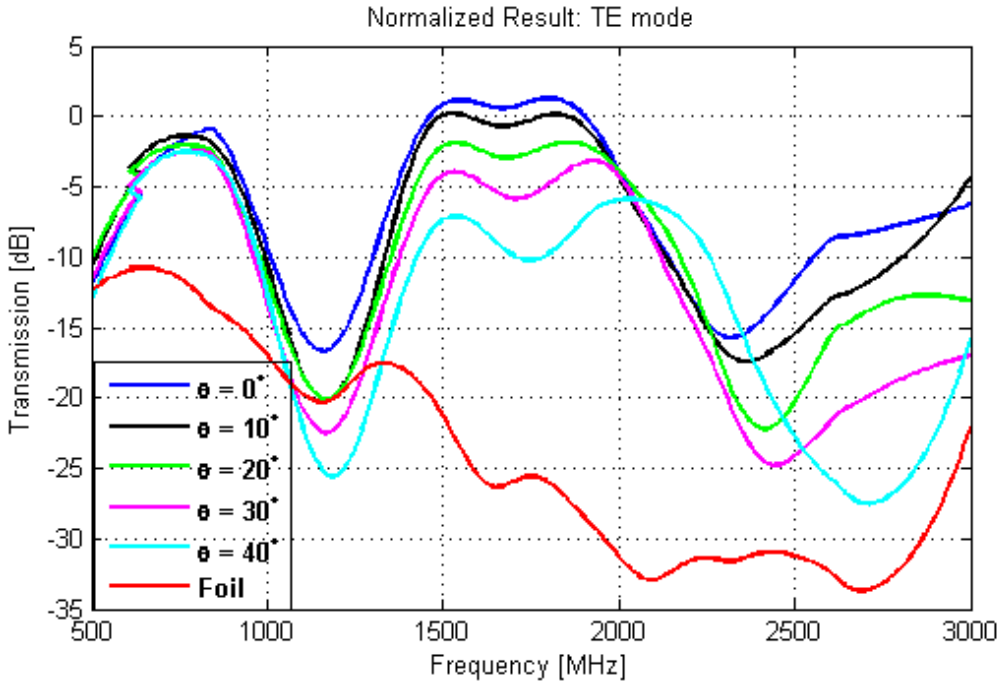

(b)

Figure 7.4. *Signal Propagation for TE mode. (a) Received signal power (b) Normalized received power. Dotted curve shows raw data and solid curve shows smoothed trend line.*

Figure 7.4 (a) shows the signal propagation through FSS at different incident angles (0° - 60°) for TE mode. The reference, which is the free space loss, is represented by yellow color. This reference is subtracted from each measured data for different incident angle to obtain the normalized result as shown in Figure 7.4 (b). Figure 7.4 (b) shows a plane aluminum foil is attenuating the signal by 14 dB at 900 MHz. The attenuation increases to 32 dB as the frequency increases to 2100 MHz. Two band-pass regions have been clearly observed, one in GSM band and one in UMTS band for every measured value. Exact resonant frequency of the upper band-pass region is difficult to figure out due to the wavy nature of peak. But the signal transmission level decreases with increasing angle of incident because the aluminum foil used for the fabrication is not PEC. It can also be seen from the Figure 7.4 (b) that the transmission level at certain frequencies is above 0 dB. It shows the FSS have few dBs gain at certain frequencies, which is not possible because FSS is a passive component and should not have gain. However, the laboratory in this measurement is not an anechoic chamber so the received signal has many multipath components which could have added constructively at particular frequency to provide gain.

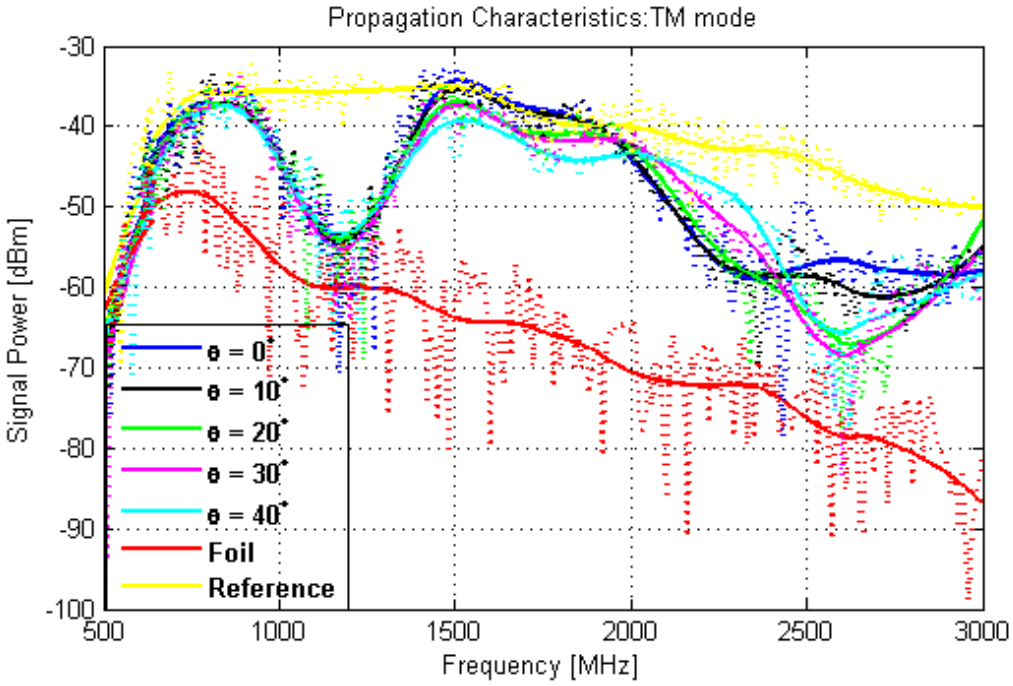

(a)

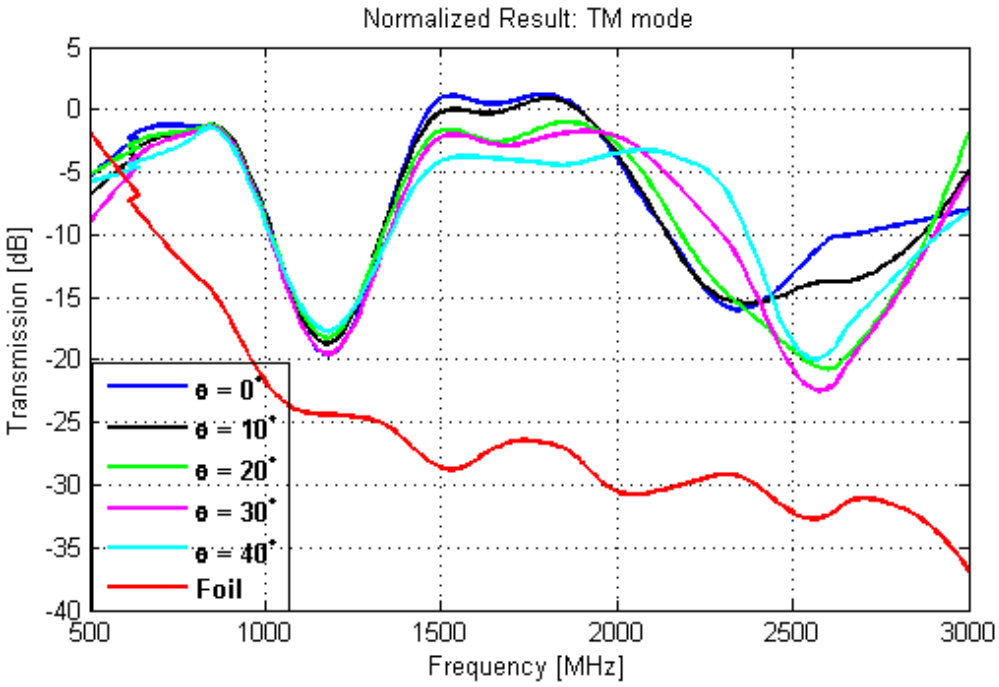

(b)

Figure 7.5. *Signal Propagation for TM mode. (a) Received signal power (b) Normalized received power. Dotted curve shows raw data and solid curve shows smoothed trend line.*

The orientation of both TX and RX antenna are rotated by 90° such that the electric field becomes parallel to the plane of incidence which is considered to be TM polarization. Similar to the TE polarization, Figure 7.5 shows the signal propagation through FSS for TM polarization. It is necessary for FSS to exhibit similar frequency filtering characteristics for both TE and TM mode because in real time application the polarization of the incoming signal varies due to multipath propagation phenomenon. Measurement results in Figure 7.4(b) and 7.5(b) show, the FSS prototype has similar characteristics for both TE and TM mode. Both band-pass regions of the FSS prototype are shifted downwards than the originally modelled freestanding FSS because of the presence of a dielectric substrate in prototype. Regardless of this frequency shift, the FSS prototype still shows reasonable improvement of signal transmission in desired frequency band compared to the plane aluminum foil. The normalized transmission levels of signal through FSS at 900 MHz, 1800 MHz and 2100 MHz for TE and TM polarization are summarized in Table 7.1.

Table 7.1. *Lab Measurement Results Summary.*

Normalized signal transmission through			Frequency					
			900 MHz		1800 MHz		2100 MHz	
			TE mode	TM mode	TE mode	TM mode	TE mode	TM mode
Foil [dB]			-14.56	-16.86	-26.03	-26.68	-32.95	-30.62
FSS at incidence angle, θ	**0°**	Measured [dB]	-2.89	-2.42	1.28	1.21	-8.48	-8.31
		Improvement [dB]	**11.67**	**14.44**	**27.31**	**27.89**	**24.47**	**22.31**
	10°	Measured [dB]	-4.97	-2.20	0.09	0.88	-8.78	-7.99
		Improvement [dB]	**9.59**	**14.66**	**26.12**	**27.56**	**24.17**	**22.63**
	20°	Measured [dB]	-4.97	-2.47	-2.09	-1.28	-6.99	-6.19
		Improvement [dB]	**9.59**	**14.39**	**23.94**	**25.4**	**25.96**	**24.43**
	30°	Measured [dB]	-5.44	-2.54	-4.86	-2.21	-8.86	-4.09
		Improvement [dB]	**9.12**	**14.32**	**21.17**	**24.47**	**24.09**	**26.53**
	40°	Measured [dB]	-4.76	-2.79	-9.79	-4.33	-6.21	-3.29
		Improvement [dB]	**9.8**	**14.07**	**16.24**	**22.35**	**26.74**	**27.33**

In Table 7.1, the signal transmission through foil is subtracted from signal transmission through FSS at each angle of incident to obtain the signal level improvement. The improvement of signal transmission through FSS compared to that of aluminum foil at different incident angle is shown in the Table 7.2.

Table 7.2. *Signal transmission improvement through FSS compared to foil.*

Incident angle, θ	**Frequency**					
	900 MHz		**1800 MHz**		**2100 MHz**	
	TE Mode	TM Mode	TE Mode	TM Mode	TE Mode	TM Mode
0°	11.67 dB	14.44 dB	27.31 dB	27.89 dB	24.47 dB	22.31 dB
10°	9.59 dB	14.66 dB	26.12 dB	27.56 dB	24.17 dB	22.63 dB
20°	9.59 dB	14.39 dB	23.94 dB	25.4 dB	25.96 dB	24.43 dB
30°	9.12 dB	14.32 dB	21.17 dB	24.47 dB	24.09 dB	26.53 dB
40°	9.8 dB	14.07 dB	16.24 dB	22.35 dB	26.74 dB	27.33 dB

Table 7.2 shows, for TE mode as the incident angle changes from 0° to 40°, the signal transmission level decreases around 2 dB at 900 MHz and around 10 dB at 1800 MHz but at 2100 MHz it increases by 2 dB. Similarly for TE mode, signal transmission level is almost constant at 900 MHz, decreases by 5 dB at 1800 MHz and increases by 5 dB at 2100 MHz. As it can be seen from the simulation results in chapter 6, the signal

transmission level variation for different incident angle at desired frequency band is very less. One of the main reasons behind such disagreement between measured and simulated results is the unknown characteristics of the aluminum foil used in prototype fabrication.

7.2.3. Comparison of Simulated and Lab Measured Results

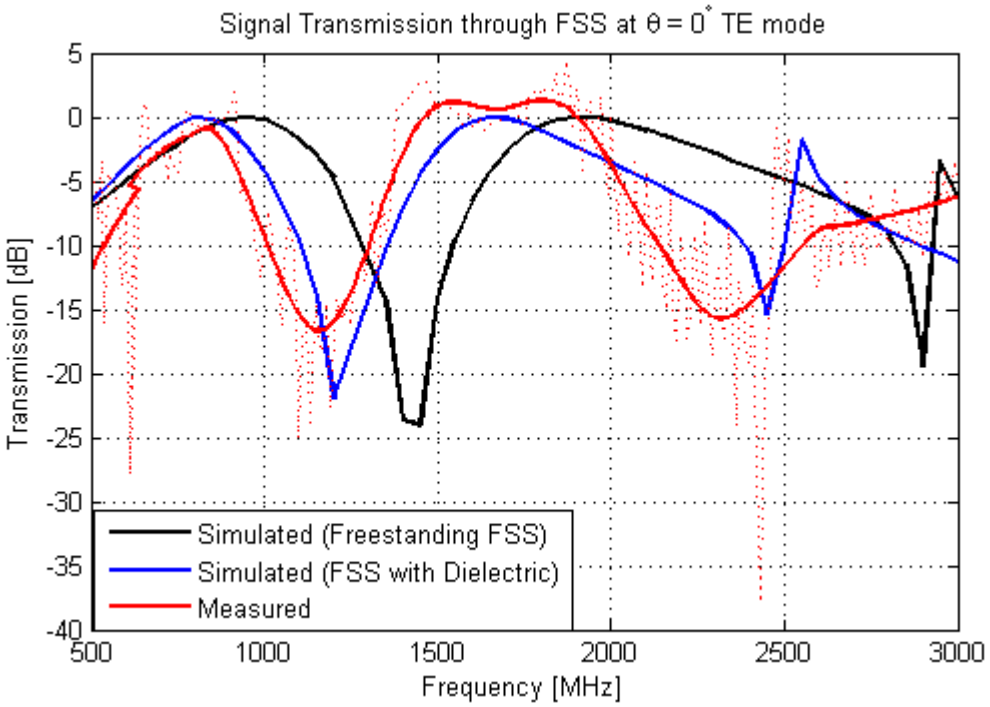

Figure 7.6. *Comparison of simulated and lab measured results.*

Figure 7.6 shows the simulated result of free-standing FSS and FSS with dielectric along with the lab measured data for TE polarization at normal incident angle. Dotted red curve shows the measured raw data and the solid red line shows the approximate smoothed curve for measured data. Measured data shows the resonant frequency has shifted downwards in both the desired frequency band comparing to the free-standing FSS simulation result. This resonant frequency shift can be best explained by the presence of plastic board which is acting as dielectric substrate on one side of FSS. The exact resonant frequency of the fabricated FSS prototype is difficult to figure out due to the uneven curve of the measured data. However, the measurement result is in good agreement with the simulated result for FSS with dielectric as predicted. Hence a conclusion can be drawn that it is very important to take the electric characteristics of dielectric substrate into consideration while designing the FSS. Even though the resonant frequency of the fabricated FSS prototype has shifted compared to the designed FSS but it still shows the transmission improvement compared to plain aluminum in the desired frequency band.

7.3. Field Measurements

The field measurement was done inside a room of the seventh floor apartment building in Lahti, Finland. This selected building represents a modern energy efficient house and has weak RF signal reception inside the building. Thus, to improve the indoor signal reception, all three operators of Finland have their own repeater inside the building. The height of service antenna of the repeater is at the second floor. So the signal should travel through multiple walls and floors before reaching the test room. The signal strength from the repeater at the test room was also very low. Hence, the repeater inside the building was turn off for all the measurements to analyze the outdoor-to-indoor RF signal propagation through FSS. Thus, the received signal at the test room was solely from the outdoor base station.

7.3.1. Description of the Test Room

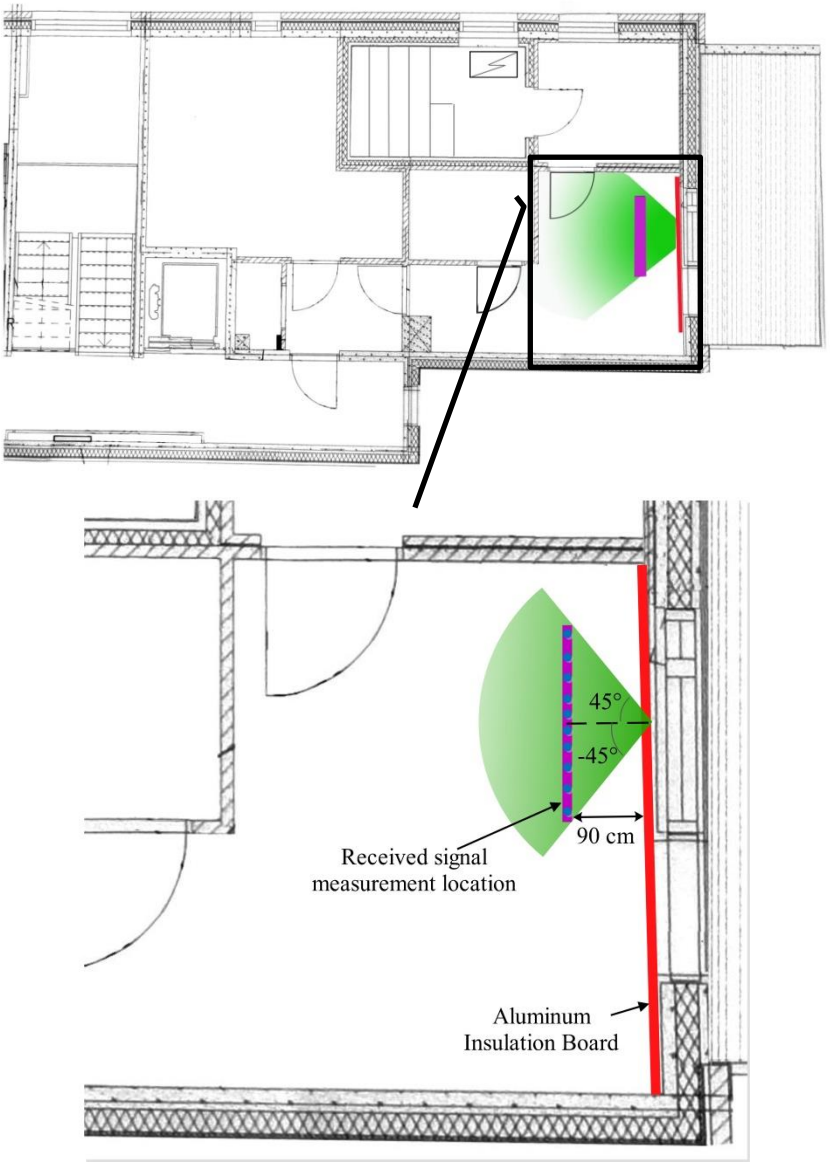

Figure 7.7. *Plan of the measurement location.*

A test room was an empty place located on the seventh floor of the apartment building. Some part of the seventh floor blueprint where the measurement was done is shown in Figure 7.7. A glass window on the reference wall was kept opened during the measurement. Then the reference wall was covered with aluminum insulation board as shown in Figure 7.7 by the red line. Aluminum foil of size 50 cm × 60 cm was cut off from the both sides of the insulation board, whose center was located 110 cm above the room floor as shown in Figure 7.8 (a). It was then replaced by aluminum foil and FSS for two different measurement scenarios. The measurement setups for aluminum foil and FSS can be seen in Figure 7.8 (b) and 7.8 (c) respectively.

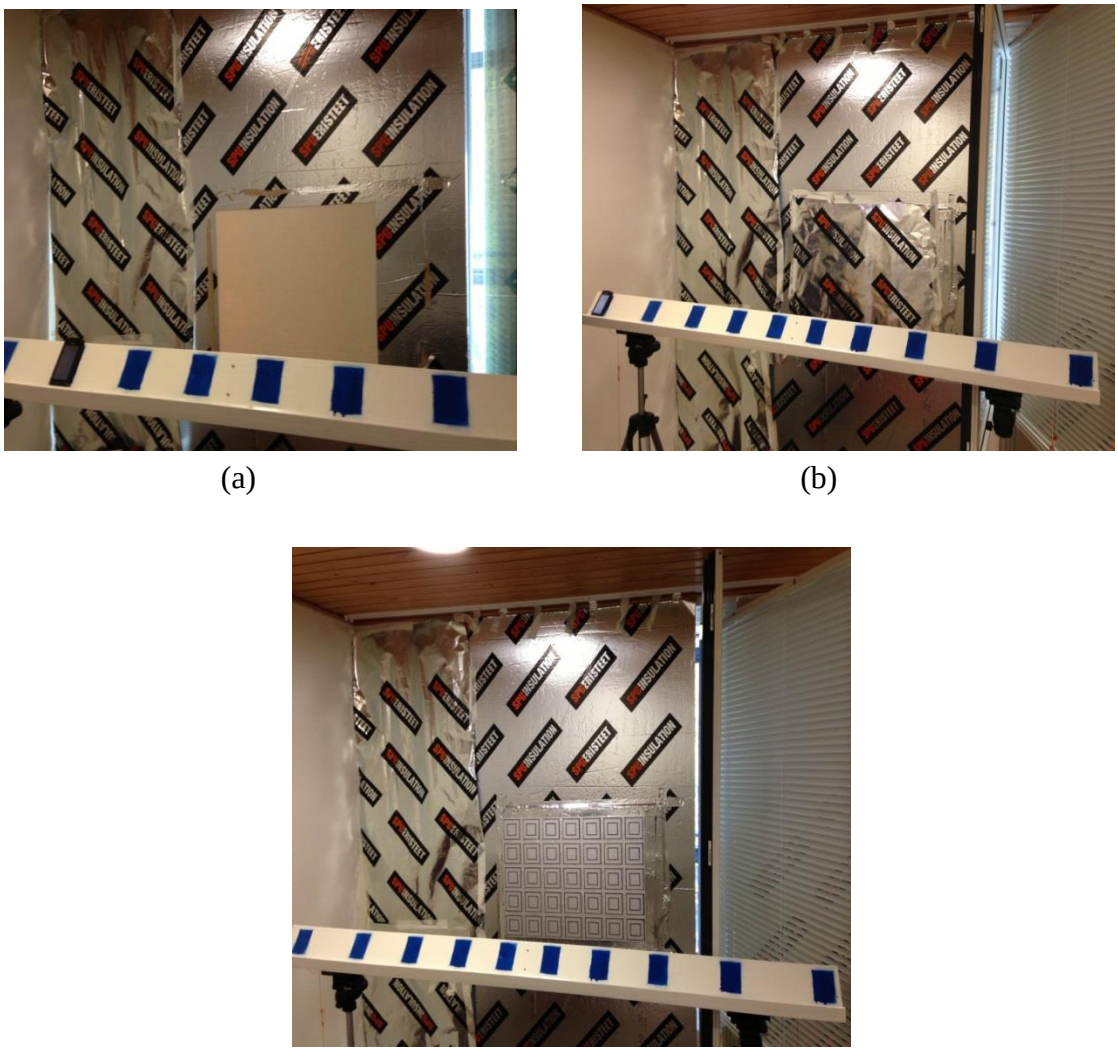

(a) (b)

(c)

Figure 7.8. *Field Measurement setup. (a) FSS size hole. (b) For aluminum foil (c) For FSS.*

RF signal strength inside a room was measured at a distance of 90 cm from the reference wall as shown in Figure 7.7. Nemo handy enabled mobile phone was used to measure the RF signal level inside the room. The measurement samples were taken at ten different positions which are marked by blue color in Figure 7.7 and 7.8. The mobile phone was placed at each measuring place for 30 seconds. The measurements were con-

ducted on two frequency bands: GSM and UMTS for all three operators (DNA, Elisa and TeliaSonera). During each measurement, active voice call was made for five minutes and the samples of received signal were collected. For the measurements at GSM band, GSM BCCH signal levels (RX LEVEL), and for UMTS band, UMTS P-CPICH levels (RSCP) were measured. The range for the angle of the incident wave varies from 0° to 45° and from 0° to -45° for the field measurement as shown in Figure 7.7. The samples of the received signals within these ranges were collected and the averaging was done.

7.3.2. Field Measurements Results

Figure 7.9 (a) shows the RX level of DNA for the GSM 900 band with the aluminum foil and the FSS. This figure shows that the RX level with the FSS has a higher value than that of the plain aluminum foil. The difference between the RX level from FSS and aluminum foil can be seen in Figure 7.9 (b). The variation in the signal is due to the constructive and destructive adding of multipath signals inside the room. The red and the black straight line in Figure 7.9 (a) are the average value of the RX level for aluminum foil and the FSS respectively. The transmission improvement of indoor received signal level of FSS over aluminum foil for DNA is around 13 dB.

Similarly, Figure 7.10 (a) shows the RSCP value of DNA through FSS and aluminum foil for UMTS 2100 MHz frequency band. RSCP value in case of FSS is clearly higher than the aluminum foil case. The difference of RSCP between FSS and aluminum foil for DNA is around 5 dB which is shown in Figure 7.10 (b).

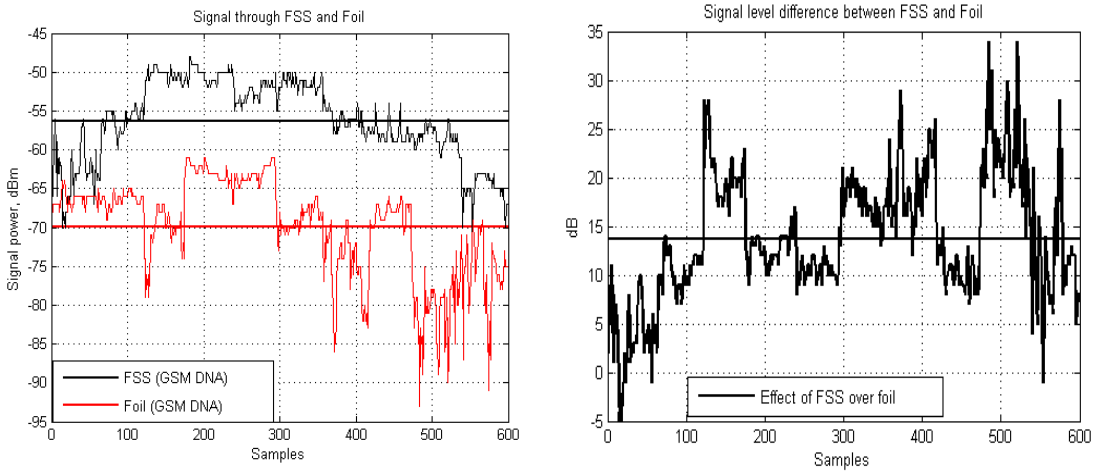

Figure 7.9. *Measurement results for GSM 900 frequency band. (a) Received signal power. (b) Signal level improvement.*

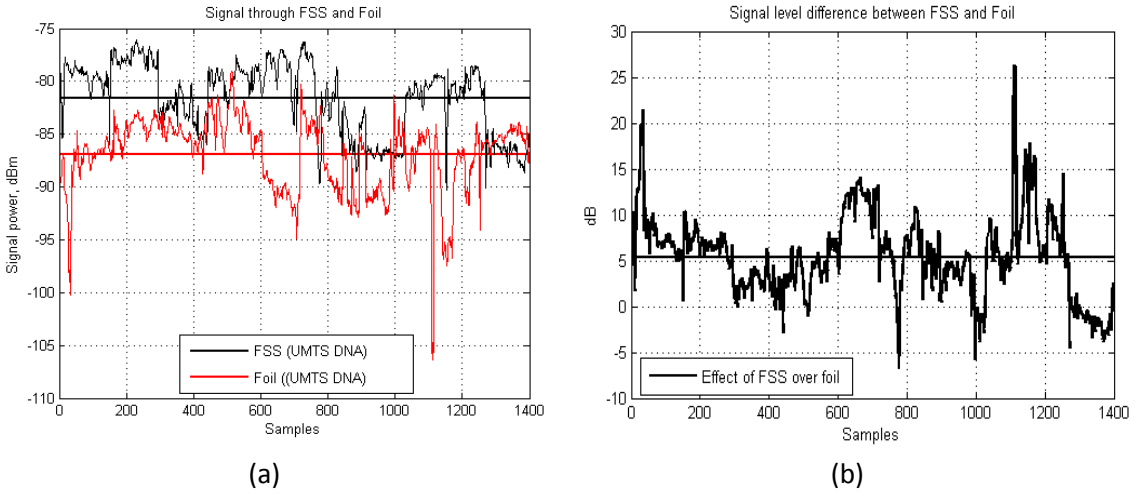

Figure 7.10. *Measurement results for UMTS 2100 frequency band. (a) Received signal power. (b) Signal level improvement.*

Similar measurement results for Elisa and TeliaSonera are presented in Appendix 1 and 2 respectively. The field measurement results for all operators will be presented in section 7.3.3.

7.3.3. Discussion of Field Measurement Results

The field measurement results were analyzed and the averaged measurement results for all three operators are summarized in the Table 7.3.

Table 7.3. *Field measurement results.*

Average Signal power through	**DNA**		**ELISA**		**TELIASONERA**	
	GSM 900	UMTS 2100	GSM 1800	UMTS 2100	GSM 900	UMTS 2100
FSS	-56.3 dBm	-81.58 dBm	-83.05 dBm	-92.12 dBm	-65.96 dBm	-78.95 dBm
Foil	-69.94 dBm	-86.92 dBm	-91.69 dBm	-97.98 dBm	-76.08 dBm	-81.41 dBm
Improvement (FSS-Foil)	**13.63 dB**	**5.34 dB**	**8.64 dB**	**5.85 dB**	**10.13 dB**	**2.46 dB**

Table 7.3 shows the average signal power through FSS and plane aluminum foil. The improvement of signal level through FSS compared to foil is calculated by subtracting the foil results from the FSS results. For DNA GSM900, Elisa GSM1800 and TeliaSonera GSM900, the transmission improvement of the radio signals through FSS over plane aluminum foil are approximately 13 dB, 8 dB and 10 dB respectively. Similarly, transmission improvement in UMTS2100 band for DNA, Elisa and TeliaSonera are approximately 5 dB, 5 dB and 2 dB respectively. The transmission improvements in

GSM band for all operators are close enough as predicted from the laboratory measurement. But, in UMTS band the use of FSS does not show significant transmission improvement. Nevertheless, field measurement results clearly show the signal transmission through FSS is better than aluminum foil. The signal transmission in GSM band is better than the UMTS band for all three operators.

7.3.4. Challenges in the Field Measurement

The reliability of the field measurement result depends on the level of signal attenuation from the building construction materials. The performance of the FSS can be seen well in the passive houses which have a high level of RF signal attenuation. The results obtained for the lab and field measurements are not exactly comparable due to the different measurement environments. The performance of the FSS in the real network is largely dependent on the location of the BS transmitter. The strength, polarization and the incident angle of the incoming signal depend on the location of the BS. As we know, the performance of the FSS starts to degrade as the angle of incident wave starts to increase. Furthermore, the BS for GSM and UMTS may be located at different places for different operators which might be a possible reason for only few dB improvements in UMTS band for all operators. All these real-time measurement environments were unknown which explain the variation of signal transmission level through FSS for different operators. In the laboratory, the TX and RX antenna are always in LOS for different incident angle measurement, but in field measurement it was not the case as the BS is fixed.

8. CONCLUSION

The objective of this thesis was to investigate the assessment of FSS for improving indoor cellular coverage. In order to meet this objective, FSS structure with double square loop aperture as unit element was selected for the analysis. The FSS structure was modelled and simulated using simulation software, CST Microwave Studio. Preliminary measurement of the modelled FSS was carried out in the laboratory of Tampere University of Technology, and the final measurement was done inside the apartment building located in Lahti, Finland. The final or the field measurement was carried out in the real network of the operators DNA, Elisa and TeliaSonera for GSM and UMTS frequency bands.

The designed FSS was able to show the transmission improvement at 900 MHz, 1800 MHz and 2100 MHz of GSM and UMTS frequency band. Regardless of unknown electric characteristic of aluminum foil and substrate, laboratory measurement result satisfies the simulation result. However, the laboratory measured data and the field measured data shows some variation due to various constraints. In the laboratory, signal strength of the transmitted signal was regulated from the signal generator. A horn antenna was used to direct the sharp beam of the plane wave through FSS. Similar horn antenna was used to collect the transmitted signal that passes through FSS. Further, in the laboratory measurement, location of the transmitter and the receivers were known and were varied accordingly for the measurements. Also, the transmitter and receiver had a clear line of sight during all measurement. Since the field measurements were done in a real network, the location of the transmitter BS was fixed somewhere. So the received signal inside a test room does not have strong LOS component rather it has only multipath components. The location of the receiver inside the test room was varied to measure the average received signal. Thus, the variation in the laboratory measurement and the field measurement can be predicted but the nature of the signal received at the receiver with the FSS is better than the signal received using aluminum foil in both the measurement. However, the field measurement result of DNA shows the transmission improvement over plain aluminum foil of 13 dB and 5 dB in GSM and UMTS frequency band respectively. Similarly, transmission improvement for Elisa is 8 dB and 5 dB and for TeliaSonera is 10 dB and 2 dB in GSM band and UMTS band respectively. Thus, these measurements clearly show that the use of FSS improves the signal reception in the energy efficient houses. Furthermore, some of the advantages of using FSS over traditional indoor coverage solutions are: it is a passive solution which means it does not require additional power source; operator independent; does not have addition-

al network configuration; suitable for single residential houses; easy installation and maintenance free.

Finally, a conclusion can be drawn from this thesis that FSS can be used to improve the indoor cellular coverage. The investigation of the FSS in this thesis is for academic purpose and is limited to GSM and UMTS frequency bands only. The research of FSS to cover the cellular telecommunication frequency bands as GSM, UMTS and LTE is still open which is very important for the real-time implementation. For the commercial propose, FSS should be designed in the metal coating of the energy efficient windows for better outdoor to indoor communication. The precise cutting mechanism of FSS structure along with the detailed information of coating layer and glass could increase the performance for frequency selective windows. Another important thing that needs to be considered for frequency selective windows is its energy efficient capability. It is obvious that the energy efficiency of window degrades as the metal coating is removed during FSS construction. So, FSS should be designed such that the least amount of metal coating is removed while preserving energy efficient characteristics of the windows. If frequency selective windows are designed and manufactured carefully, it can improve the indoor cellular coverage problem without additional network architecture. Hence the use of FSS, in energy saving window, could eventually lead to future radio friendly passive houses.

REFERENCES

[1] European Commission, “A policy framework for climate and energy in the period from 2020 to 2030”, COM (2014) 15 final, Brussels, 22.1.2014.

[2] European Commission’s Market Observatory for Energy, “2009 Annual Report of the Market Observatory for Energy”, Luxembourg, 2010, ISBN 978-92-79-14175-1.

[3] Andreas H., Lorenzo P., Karsten V. et.all, “Towards nearly zero-energy buildings: Definition of common principles under the EPBD”, Project no. BESDE10788, Ecofys Germany GmbH, 14.2.2013.

[4] William C. Stone, “Electromagnetic Signal Attenuation in construction Materials”, NIST Construction Automation Program Report No. 31997, USA, 1997.

[5] Ari Asp, Yaroslav Sydorov, Mikko Valkama, Jarno Niemelä, “Radio Signal Propagation and Attenuation measurements for Morden Residential Buildings’’, In: GC 2012 workshop: The 4th IEEE International workshop on Heterogeneous and Small Cell Networks. IEEE (2012).

[6] G.H.H. Sung, K.W. Sowerby, A.G. Williamson, “The impact of frequency selective surfaces applied to standard wall construction materials”, International Symposium on Antennas and Propagation, 2004.

[7] M. Raspopoulos, S. Stavrou, “Frequency Selective Buildings through Frequency Selective Surfaces” IEEE Transactions on Antennas and Propagation, 2011.

[8] G.I. Kiani, A. Karlsson, L. Olsson, K.P. Esselle, “Glass Characterization for Designing Frequency Selective Surfaces to Improve Transmission through Energy Saving Glass Windows”, APMC Microwave Conference, 2007.

[9] B. Widenberg, S. Poulsen, and A. Karlsson, “The design of window panes with high transmission at 900 MHz and 1800 MHz,” in Antenna 00, Nordic Antenna Symposium, Lund, Sweden, pp. 185–190, 2000.

[10] J.C. Batchelor, E.A. Parker, B. Sanz-Izquierdo, J.B. Robertson, I.T. Ekpo and A.G. Williamson, “Designing FSS for Wireless Propagation Control within Buildings,” Antennas & Propagation Conference, Loughborough, 2009.

[11] T.K. Wu, “Frequency Selective Surface and Grid Array’’, John Wiley and Sons, Inc., 1995, ISBN 0-471-31189-8.

[12] Simon R. Saunders and Alejandro Arajon Zavala, ‘Antennas and Propagation for Wireless Communication Systems’ Second edition, John Wiley & Sons, Ltd., 2007, ISBN: 978-0-470-84879-1.

[13] J.D. Parsons, ‘The Mobile Radio Propagation Channel’, Second Edition, John Wiley & Sons Ltd., 2000, ISBN: 978-0-471-98857-1.

[14] D. K. Cheng, “Field and Wave Electromagnetics,” 2nd ed. Addison-Wesley Publishing Company, Inc., United States of America, 1992, ISBN 0-201-01239-1.

[15] W. L. Stutzman and G. A. Thiele, “Antenna Theory and Design,” Second edition, John Wiley & Sons Inc., United States of America, 1998, ISBN 0-471-04458-X.

[16] David M. Pozar, “Microwave Engineering’’, Third edition, John Wiley & Sons,Inc., ISBN 0-471-44878-8, 205.

[17] Yi Huang and Kevin Boyle, “Antennas: From Theory to Practice’’, John Wiley & Sons, Inc., U.K., ISBN 978-0-470-51028-5, 2008.

[18] C.A. Balanis, “Antenna theory, Analysis and Design’’, Third Edition, John Wiley & Sons, Inc., New York, 2005, ISBN 978-0-470-51028-5.

[19] J.D. Kraus, “Antennas’’, Second edition, Tata McGraw-Hill Publishing Company Ltd., New Delhi, 1997, ISBN 0-07-035422-7.

[20] Theodore S. Rappaport, “Wireless Communications-Principles and Practice’’, Second Edition, Prentice-Hall, Inc. 2002, ISBN 0-13-042232-0.

[21] Morten Tolstrup, “Indoor Radio Planning: A Practical Guide for GSM, DCS, UMTS and HSPA’’, John Wiley & Sons, Ltd., 2008, ISBN 978-0-470-05769-8 (HB).

[22] Asha Mehrotra, “GSM System Engineering’’, Artech House, Inc., 1997, ISBN 9780890068601.

[23] J. Lempiäinen and M. Manninen, “Radio interface system planning for GSM/GPRS/UMTS’’, Kluwer Academic Publishers, 2001, ISBN 0-7923-7516-5.

[24] GSM 05.05, “Digital cellular telecommunication system (Phase 2); Radio transmission and reception’’, version 5.0.0, ETSI, 1996.

[25] GSM 05.02, “Digital cellular telecommunication system (Phase 2); Multiplexing and multiple access on the radio path’’, version 5.0.0, ETSI, 1996.

[26] Holma, H and Toskala, “WCDMA for UMTS: HSPA Evolution and LTE’’, John Wiley & Sons Ltd, Fourth Edition, Sept.27, 2007, ISBN 978-0-470-31933-8 (HB).

[27] Heikki Kaaranen, Ari Ahtiainen, Lauri Laitinen, Siamäk Naghian and Valtteri Niemi, “UMTS Networks: Architecture, Mobility and Services’’, Second edition, John Wiley & Sons Ltd. 2005, ISBN 0-470-01103-3.

[28] Finnish Communications Regulatory Authority. [Accessed on 30.1.2014]. Available at: https://www.viestintavirasto.fi/ohjausjavalvonta/lupapaatokset/radiolupapaatokset.html.

[29] Andreas F. Molisch, “Wireless Communications’’, Second Edition, John Wiley & Sons Ltd., 2011, ISBN: 978-0-470-74186-3.

[30] Antti V. Räisänen, Arto Lehto; “Radio Engineering for Wireless Communication and Sensor Applications’’; Artech House; ISBN 1-58053-542-9; 2003.

[31] Simon R. Saunders and Alejandro Arajon Zavala, “Antennas and Propagation for Wireless Communication Systems’’, Second Edition, John Wiley & Sons, Ltd., 2007, ISBN 978-0-470-84879-1.

[32] J.D. Parsons, “The Mobile Radio Propagation Channel’’, Second Edition, John Wiley & Sons Ltd., 2000, ISBN 0-471-98857-X.

[33] Nathan Blaunstein and Christos Christodoulou, “Radio Propagation and Adaptive Antennas for Wireless Communication Links’’, John Wiley & Sons, Inc., 2007, ISBN: 978-0-471-25121-7.

[34] Tero Isotalo, “Indoor Planning in Broadband Cellular Radio Networks’’, Tampere University of Technology, Tampere 2012, ISBN 978-952-15-2964-1.

[35] Hui-Hsia Sung, “Frequency Selective Wallpaper for Mitigating Indoor Wireless Interference’’, University of Auckland, 2006.

[36] Salvatore Celozzi, Rodolfo Araneo and Giampiero Lovat, “Electromagnetic Shielding’’ John Wiley & Sons, Inc., 2008, ISBN: 978-0-470-05536-6.

[37] Constantine A. Balanis, “Modern Antenna Handbook’’, John Wiley & Sons, Inc., 2008, ISBN: 9780470036341.

[38] C. Mias, C. Tsakonas and C. Oswald, “An Investigation into the Feasibility of designing Frequency Selective Windows employing periodic structures (Ref. AY3922)’’, Final Report for the Radio communications Agency, The Nottingham Trent University, U.K.

[39] Ben A. Munk, “Frequency Selective Surfaces: Theory and Design’’, John Wiley & Sons, Inc., New York, 2000, ISBN 0-471-37047-9 (alk. Paper).

[40] Zhong Ming Tan and Kirk T. McDonald, “Babinet’s Principle for Electromagnetic Fields’’ Joseph Henry Laboratories, Princeton University, January 19, 2012.

[41] B.A. Munk, R. Kouyoumjian, and L. Peters Jr., “Reflection Properties of Periodic Surfaces of Loaded Dipoles,” IEEE Transactions on Antennas and Propagation, vol. AP-19, pp. 612-617, September 1971.

[42] John David Shumpert, “Modelling of Periodic Dielectric Structures (Electromagnetic Crystals)’’, University of Michigan, 2001.

[43] Marios Raspopoulos and Stavros Stavrou, “Frequency Selective Buildings Through Frequency Selective Surfaces’’, IEEE Tansactions on Antennas and Propagation, vol. 59, no. 8, August 2011.

[44] U. Rafique, M. M. Ahmed, M. A. Haq and M. T. Rana, “Transmission of RF Signals through Energy Efficient Window Using FSS”, Emerging Technologies (ICET), Seventh International Conference, 2011.

[45] N. Marcuvitz, “Waveguide Handbook’’, Peter Peregrinus Ltd., New York 1986.

[46] P. Callaghan, E. A. Parker, and R. J. Langley, “Influence of supporting dielectric layers on the transmission properties of frequency selective surfaces”, Micro-

wave Antennas and Propagation, IEE Proceedings H, vol. 138, no. 5, pp. 448–454, 1991.

[47] CST Microwave Studio 2012, [accessed on 5.2.2014]. Available at: https://www.cst.com/Contents/Products/MWS/Overview.aspx.

[48] Mohan Jayawardene and Yiannis Vardaxoglou, "3-D EM Simulation of Infinite Periodic Arrays and Finite Frequency Selective Horns'', ARMMS conferences, April 2006.

[49] G.I. Kiani, A. Karlsoon, L. Osslon, K.P. Esselle, and M. Nilson, "Transmission of infrared and visible wavelengths through energy-saving glass due to etching of frequency selective surfaces", IET Microwaves, Antennas, and Propagation, vol. 4, no. 7, July 2010.

[50] Irfan Ullah, Xiaoli Zhao, Daryoush Habibi and Ghaffer Kiani, "Transmission Improvement of UMTS and Wi-Fi Signals Through Energy Saving Glass Using FSS'', 2011.

[51] Ghaffer I. Kiani, Lars G. Olsson, Anders Karlsson, Karu P. Esselle and Martin Nilsoon, "Cross-Dipole Bandpass Frequency Selective Surface for Energy-Saving Glass Used in Buildings", IEEE Transactions on Antennas and Propagation, vol. 59, no. 2, February 2011.

[52] Irfan Ullah, Xiaoli Zhao, Daryoush Habibi and Ghaffer Kiani, "Transmission Improvement of UMTS and Wi-Fi Signals Through Energy Saving Glass Using FSS", Wireless and Microwave Technology Conference (WAMICON), 2011.

APPENDIX 1: FIELD MEASUREMENT FOR ELISA

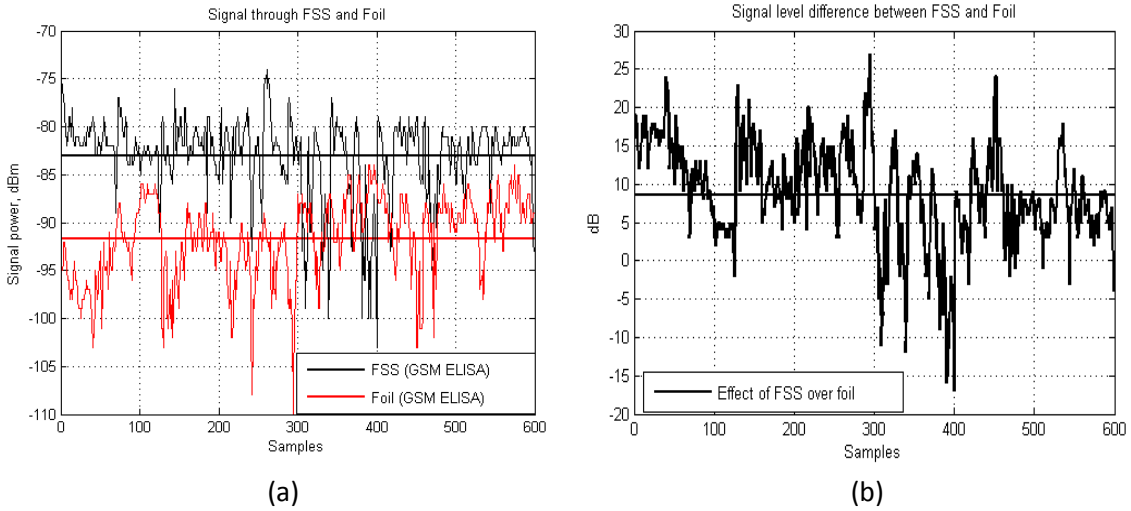

Figure A1.1. *Measurement results for GSM 1800 frequency band. (a) Received signal power. (b) Signal level improvement.*

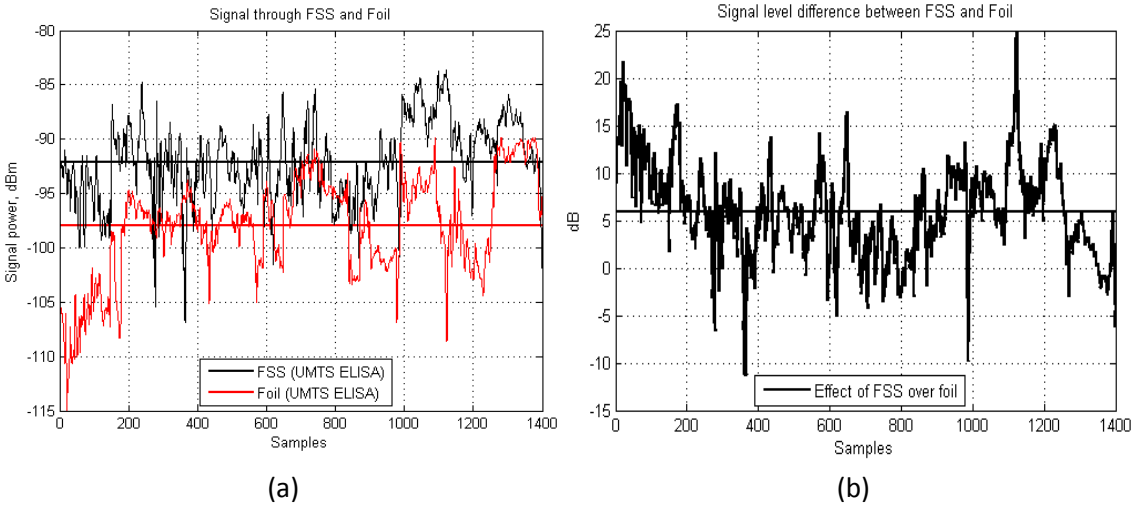

Figure A1.2. *Measurement results for UMTS 2100 frequency band. (a) Received signal power. (b) Signal level improvement.*

APPENDIX 2: FIELD MEASUREMENT FOR TELIASONERA

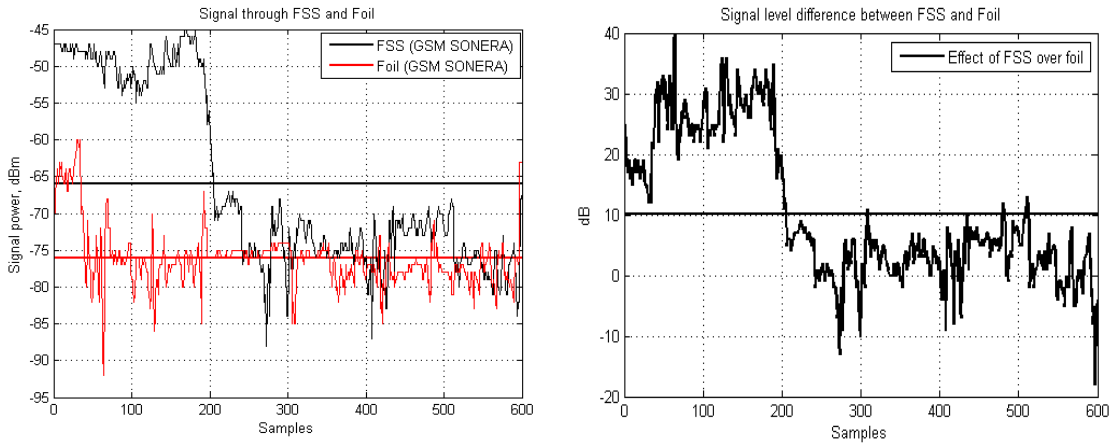

(a) (b)

Figure A2.1. *Measurement results for GSM 900 frequency band. (a) Received signal power. (b) Signal level improvement.*

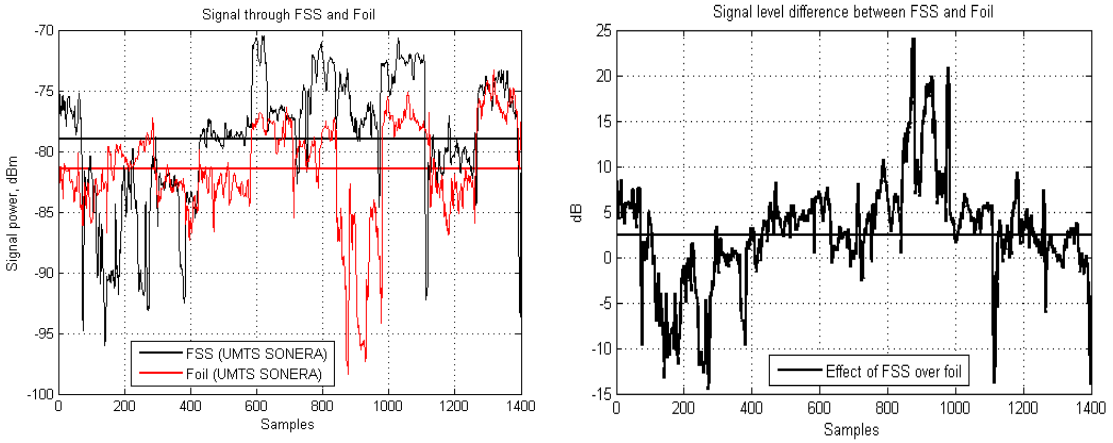

(a) (b)

Figure A2.2. *Measurement results for UMTS 2100 frequency band. (a) Received signal power. (b) Signal level improvement.*